

Fig. 2. Specific contribution of TLR3 to XMRV-induced IP-10/CXCL10. (A) Inhibition of IP-10/CXCL10 production by a dominant-negative derivative of TLR3 (dnTLR3). The dnTLR3 was transfected into LNCaP cells by MuLV vector and the cells were selected with puromycin. The constitutive expression of dnTLR3 in LNCaP cells was verified by Western blot analysis (upper panel). Actin was used as the internal control. The TLR3 ligand and XMRV infection failed to upregulate production of IP-10/CXCL10 by cells expressing dnTLR3 (lower panel). The error bar represents the SD of triplicated wells. Representative data from three independent experiments are shown. Statistical significance was detected between ligand-exposed or XMRV-infected control cells and each of the other groups by two-tailed Student's *t*-test (asterisk, $P < 0.01$). (B) Inhibition of XMRV-induced IP-10/CXCL10 production by a TLR3 inhibitor. The RNA isolated from LNCaP cells infected with XMRV in the presence or absence of the TLR3 inhibitor 4a (10 and 25 μM) was subjected to RT-PCR designed to detect IP-10/CXCL10 mRNA. GAPDH was used as the internal control. Representative data from three independent experiments are shown.

to infect cells because retroviruses are intrinsically unstable due to the loss of Env function [33]. Such defective viruses should be degraded in the endosome where the genomic RNA from these viral particles could be exposed to the host RNA sensors, including TLR3. The “endosome model” can be tested by using endosomal acidification inhibitors as reported by Beignon et al. [1]. However, this experimental approach was not possible in our experimental setting because IP-10/CXCL10 production was attenuated by such inhibitors, including Chloroquine or Bafilomycin A1. Retrovirus is an enveloped virus. Thus, the genomic RNA of XMRV should not be exposed to the surface of the virion. It appears unlikely, therefore, that the recognition of viral genomic RNA by TLR3 takes place at the cell surface unless TLR3 recognizes non-nucleic acid component on the surface of XMRV particle.

The historical studies on recognition of retroviruses by TLRs did not assess the involvement of a newly-identified PRR, TRIM5 [22]. In our experimental system, this potential caveat is clarified because human TRIM5 does not restrict XMRV entry [21,22]. The contribution of TLR3 to the recognition of retroviruses could have been difficult to detect partly because the expression levels of TLR7 might be higher than those of TLR3 in that experimental system, or that the TLR3-induced signal might not have been robust

enough to detect. Thus, the failure of TLR3 signal detection does not necessarily mean that retroviruses do not activate the TLR3 signal. In the study by Breckpot et al. [34], activation of the TLR signal depended on reverse transcription of the viral genome using a replication-defective HIV-1-based lentiviral vector in mouse-derived dendritic cells. The reverse transcription of retroviral genome is considered to take place in the cell cytoplasm. Thus, the molecular sensor that recognizes the reverse-transcribed nucleic acid should be present in the cytoplasm, not in the endosomal compartment. The activation of anti-viral signal reported by Breckpot et al. should be, therefore, TLR3-independent. More recently, Kane et al. reported that MMTV and MuLV activate humoral responses via the TLR7 signal in mouse [10]. This, again, does not necessarily prove that TLR3 is not activated by these retroviruses, for it was noted that some immune responses were evoked by retroviral infection in a TLR7-independent manner. Although TLR7 serves as a front line, the TLR3 may be the second line PRR-mediated host defense against retroviruses. The *in vivo* relevance of TLR3 activation by retroviruses remains to be clarified in future studies.

Acknowledgments

K.M., E.U., S.T., T.M., Y.O., K.C., H.Y., M.K., and J.K. designed and performed the experiments and interpreted the data. J.K., E.U. and K.M. wrote the manuscript. This work was supported by the Japan Health Science Foundation, the Japanese Ministry of Health, Labor, and Welfare, and the Japanese Ministry of Education, Culture, Sports, Science and Technology. All authors declare no potential competing financial interests.

References

- [1] K. Brennan, A.G. Bowie, Activation of host pattern recognition receptors by viruses, *Curr. Opin. Microbiol.* 13 (2010) 503–507.
- [2] T. Kawai, S. Akira, The role of pattern-recognition receptors in innate immunity: update on Toll-like receptors, *Nat. Immunol.* 11 (2010) 373–384.
- [3] M.E. Kleinman, K. Yamada, A. Takeda, et al., Sequence- and target-independent angiogenesis suppression by siRNA via TLR3, *Nature* 452 (2008) 591–597.
- [4] X. Guo, J.W. Carroll, M.R. Macdonald, et al., The zinc finger antiviral protein directly binds to specific viral mRNAs through the CCCH zinc finger motifs, *J. Virol.* 78 (2004) 12781–12787.
- [5] D. Wolf, S.P. Goff, Embryonic stem cells use ZFP809 to silence retroviral DNAs, *Nature* 458 (2009) 1201–1204.
- [6] M.K. Lewinski, F.D. Bushman, Retroviral DNA integration—mechanism and consequences, *Adv. Genet.* 55 (2005) 147–181.
- [7] A.S. Beignon, K. McKenna, M. Skoberne, et al., Endocytosis of HIV-1 activates plasmacytoid dendritic cells via Toll-like receptor-viral RNA interactions, *J. Clin. Invest.* 115 (2005) 3265–3275.
- [8] A.W. Hardy, D.R. Graham, G.M. Shearer, et al., HIV turns plasmacytoid dendritic cells (pDC) into TRAIL-expressing killer pDC and down-regulates HIV coreceptors by Toll-like receptor 7-induced IFN- α , *Proc. Natl. Acad. Sci. USA* 104 (2007) 17453–17458.
- [9] S.I. Gringhuis, M. van der Vliet, L.M. van den Berg, et al., HIV-1 exploits innate signaling by TLR8 and DC-SIGN for productive infection of dendritic cells, *Nature* 11 (2010) 419–426.
- [10] M. Kane, L.K. Case, C. Wang, et al., Innate immune sensing of retroviral infection via toll-like receptor 7 occurs upon viral entry, *Immunity* 2011 (2011) 29.
- [11] A. Lepelletier, S. Louis, M. Sourisseau, et al., Innate sensing of HIV-infected cells, *PLoS* 7 (2011) e1001284.
- [12] R. Colisson, L. Barblu, C. Gras, F. Raynaud, R. Hadj-Slimane, C. Pique, O. Hermine, Y. Lepelletier, J.P. Herbeval, Free HTLV-1 induces TLR7-dependent innate immune response and TRAIL relocalization in killer plasmacytoid dendritic cells, *Blood* 115 (2010) 2177–2185.
- [13] R.S. Russell, C. Liang, M.A. Wainberg, Is HIV-1 RNA dimerization a prerequisite for packaging? Yes, no, probably?, *Retrovirology* 1 (2004) 23.
- [14] J. Grotorex, The retroviral RNA dimer linkage: different structures may reflect different roles, *Retrovirology* 1 (2004) 22.
- [15] J.M. Watts, K.K. Dang, R.J. Gorelick, et al., Architecture and secondary structure of an entire HIV-1 RNA genome, *Nature* 460 (2009) 711–716.
- [16] K. Cheng, X. Wang, H. Yin, Small-molecule inhibitors of the TLR3/dsRNA complex, *J. Am. Chem. Soc.* 133 (2011) 3764–3767.
- [17] J. Komano, K. Miyauchi, Z. Matsuda, et al., Inhibiting the Arp2/3 complex limits infection of both intracellular mature vaccinia virus and primate lentiviruses, *Mol. Biol. Cell* 15 (2004) 5197–5207.

- [18] S. Shimizu, E. Urano, Y. Futahashi, et al., Inhibiting lentiviral replication by HEXIM1, a cellular negative regulator of the CDK9/cyclin T complex, *AIDS* 21 (2007) 575–582.
- [19] R. Galli, D. Starace, R. Busa, et al., TLR stimulation of prostate tumor cells induces chemokine-mediated recruitment of specific immune cell types, *J. Immunol.* 184 (2010) 6658–6669.
- [20] M.J. Metzger, C.J. Holguin, R. Mendoza, A.D. Miller, et al., The prostate cancer-associated human retrovirus XMRV lacks direct transforming activity but can induce low rates of transformation in cultured cells, *J. Virol.* 84 (2010) 1874–1880.
- [21] H.C. Groom, M.W. Yap, R.P. Galao, S.J. Neil, et al., Susceptibility of xenotropic murine leukemia virus-related virus (XMRV) to retroviral restriction factors, *Proc. Natl. Acad. Sci. USA* 107 (2010) 5166–5171.
- [22] T. Pertel, S. Hausmann, D. Morger, S. Zuger, et al., TRIM5 is an innate immune sensor for the retrovirus capsid lattice, *Nature* 472 (2011) 361–365.
- [23] A. Pichlmair, S.S. Diebold, S. Gschmeissner, et al., Tubulovesicular structures within vesicular stomatitis virus G protein-pseudotyped lentiviral vector preparations carry DNA and stimulate antiviral responses via Toll-like receptor 9, *J. Virol.* 81 (2007) 539–547.
- [24] E.C. Knouf, M.J. Metzger, P.S. Mitchell, et al., Multiple integrated copies and high-level production of the human retrovirus XMRV (xenotropic murine leukemia virus-related virus) from 22Rv1 prostate carcinoma cells, *J. Virol.* 83 (2009) 7353–7356.
- [25] D. Burzyn, J.C. Rassa, D. Kim, et al., Toll-like receptor 4-dependent activation of dendritic cells by a retrovirus, *J. Virol.* 78 (2004) 576–584.
- [26] G.P. Dunn, K.C. Sheehan, L.J. Old, et al., IFN unresponsiveness in LNCaP cells due to the lack of JAK1 gene expression, *Cancer Res.* 65 (2005) 3447–3453.
- [27] J.J. Rodriguez, S.P. Goff, Xenotropic murine leukemia virus-related virus establishes an efficient spreading infection and exhibits enhanced transcriptional activity in prostate carcinoma cells, *J. Virol.* 84 (2009) 2556–2562.
- [28] B.P. Doehle, F. Hladik, J.P. McNevin, et al., Human immunodeficiency virus type 1 mediates global disruption of innate antiviral signaling and immune defenses within infected cells, *J. Virol.* 83 (2009) 10395–10405.
- [29] S. Bhosle, S. Suppiah, R. Molinaro, et al., Evaluation of cellular determinants required for in vitro xenotropic murine leukemia virus-related virus entry into human prostate cancer and noncancerous cells, *J. Virol.* 84 (2010) 6288–6296.
- [30] K. Kariko, P. Bhuyan, J. Capodici, et al., Small interfering RNAs mediate sequence-independent gene suppression and induce immune activation by signaling through toll-like receptor 3, *J. Immunol.* 172 (2004) 6545–6549.
- [31] L. Alexopoulou, A.C. Holt, R. Medzhitov, et al., Recognition of double-stranded RNA and activation of NF-kappaB by Toll-like receptor 3, *Nature* 413 (2001) 732–738.
- [32] H. Kamiyama, K. Kakoki, H. Yoshii, et al., Infection of XC cells by MLVs and Ebola virus is endosome-dependent but acidification-independent, *PLoS One* 6 (2011) e26180.
- [33] S. Andreadis, T. Lavery, H.E. Davis, et al., Toward a more accurate quantitation of the activity of recombinant retroviruses: alternatives to titer and multiplicity of infection, *J. Virol.* 74 (2000) 3431–3439.
- [34] K. Breckpot, D. Escors, F. Arce, et al., HIV-1 lentiviral vector immunogenicity is mediated by Toll-like receptor 3 (TLR3) and TLR7, *J. Virol.* 84 (2010) 5627–5636.

Neutrophil Extracellular Traps Mediate a Host Defense Response to Human Immunodeficiency Virus-1

Tatsuya Saitoh,^{1,2} Jun Komano,^{4,7} Yasunori Saitoh,⁵ Takuma Misawa,^{1,2} Michihiro Takahama,^{1,2} Tatsuya Kozaki,^{1,2} Takuya Uehata,^{1,2} Hidenori Iwasaki,^{1,2} Hiroko Omori,³ Shoji Yamaoka,⁵ Naoki Yamamoto,⁶ and Shizuo Akira^{1,2,*}

¹Laboratory of Host Defense, WPI Immunology Frontier Research Center

²Department of Host Defense, Research Institute for Microbial Diseases

³Central Instrumentation Laboratory, Research Institute for Microbial Diseases

Osaka University, 3-1 Yamada-oka, Suita, Osaka 565-0871, Japan

⁴National Institute of Infectious Diseases, 1-23-1 Toyama, Shinjuku-ku, Tokyo 162-8640, Japan

⁵Department of Molecular Virology, Graduate School of Medical and Dental Sciences, Tokyo Medical and Dental University, 1-5-45 Yushima, Bunkyo-ku, Tokyo 113-8519, Japan

⁶Department of Microbiology, Yong Loo Lin School of Medicine, National University of Singapore, Block MD4A, 5 Science Drive 2, 117597, Singapore

⁷Present address: Division of Virology, Department of Infectious Diseases, Osaka Prefectural Institute of Public Health,

1-3-69 Nakamichi Higashinari-ku, Osaka 537-0025, Japan

*Correspondence: sakira@biken.osaka-u.ac.jp

<http://dx.doi.org/10.1016/j.chom.2012.05.015>

SUMMARY

Neutrophils contribute to pathogen clearance by producing neutrophil extracellular traps (NETs), which are genomic DNA-based net-like structures that capture bacteria and fungi. Although NETs also express antiviral factors, such as myeloperoxidase and α -defensin, the involvement of NETs in antiviral responses remains unclear. We show that NETs capture human immunodeficiency virus (HIV)-1 and promote HIV-1 elimination through myeloperoxidase and α -defensin. Neutrophils detect HIV-1 by Toll-like receptors (TLRs) TLR7 and TLR8, which recognize viral nucleic acids. Engagement of TLR7 and TLR8 induces the generation of reactive oxygen species that trigger NET formation, leading to NET-dependent HIV-1 elimination. However, HIV-1 counteracts this response by inducing C-type lectin CD209-dependent production of interleukin (IL)-10 by dendritic cells to inhibit NET formation. IL-10 suppresses the reactive oxygen species-dependent generation of NETs induced upon TLR7 and TLR8 engagement, resulting in disrupted NET-dependent HIV-1 elimination. Therefore, NET formation is an antiviral response that is counteracted by HIV-1.

INTRODUCTION

Neutrophils play a pivotal role in the elimination of pathogens invading a host (Papayannopoulos and Zychlinsky, 2009). Recent studies have revealed that neutrophils undergo suicide that is beneficial for host defense, releasing net-like structures into the extracellular space to prevent the spreading of bacteria

and fungi (Brinkmann et al., 2004; Urban et al., 2009). The extracellular structures are composed of genomic DNA and histones, and are designated neutrophil extracellular traps (NETs) (Brinkmann et al., 2004). Mitochondrial DNA is also a component of NETs (Yousefi et al., 2009). Eosinophils and mast cells also produce DNA-based NET-like structures to prevent the spreading of bacteria (von Köckritz-Blickwede et al., 2008; Yousefi et al., 2008).

Reactive oxygen species (ROS) and mitogen-activated protein kinase (MAPK) mediate NET formation induced by phorbol myristate acetate (PMA), a potent inducer of NET formation (Fuchs et al., 2007; Papayannopoulos et al., 2010; Hakkim et al., 2011). MAPK activates nicotinamide adenine dinucleotide phosphate (NADPH) oxidase to induce ROS generation in response to PMA. ROS damage the membrane of secretory granules and lysosomes, and induce the translocation of neutrophil elastase from these organelles to the nucleus. Neutrophil elastase then promotes the cleavage of histones, leading to chromatin release into the cytosol.

NETs are highly sticky and capture extracellular microbes such as bacteria and fungi (Brinkmann et al., 2004; Urban et al., 2009). Furthermore, various antimicrobial factors, such as cathelicidin, calprotectin, myeloperoxidase (MPO), and α -defensin, are expressed on NETs to mediate the NET-dependent elimination of bacteria and fungi (Brinkmann et al., 2004; Urban et al., 2009). Although the pathological role of NETs remains to be elucidated, NET formation is potently induced in lungs of mice infected with influenza A virus and is affected in neutrophils isolated from cats infected with feline immunodeficiency virus (Wardini et al., 2010; Hemmers et al., 2011; Narasaraju et al., 2011).

Human immunodeficiency virus (HIV)-1 belongs to the lentivirus subfamily of retroviruses and infects human CD4⁺ T cells and human macrophages (Haseltine, 1988). HIV-1 infection disrupts the effectiveness of the human immune system and renders hosts susceptible to opportunistic infections, leading

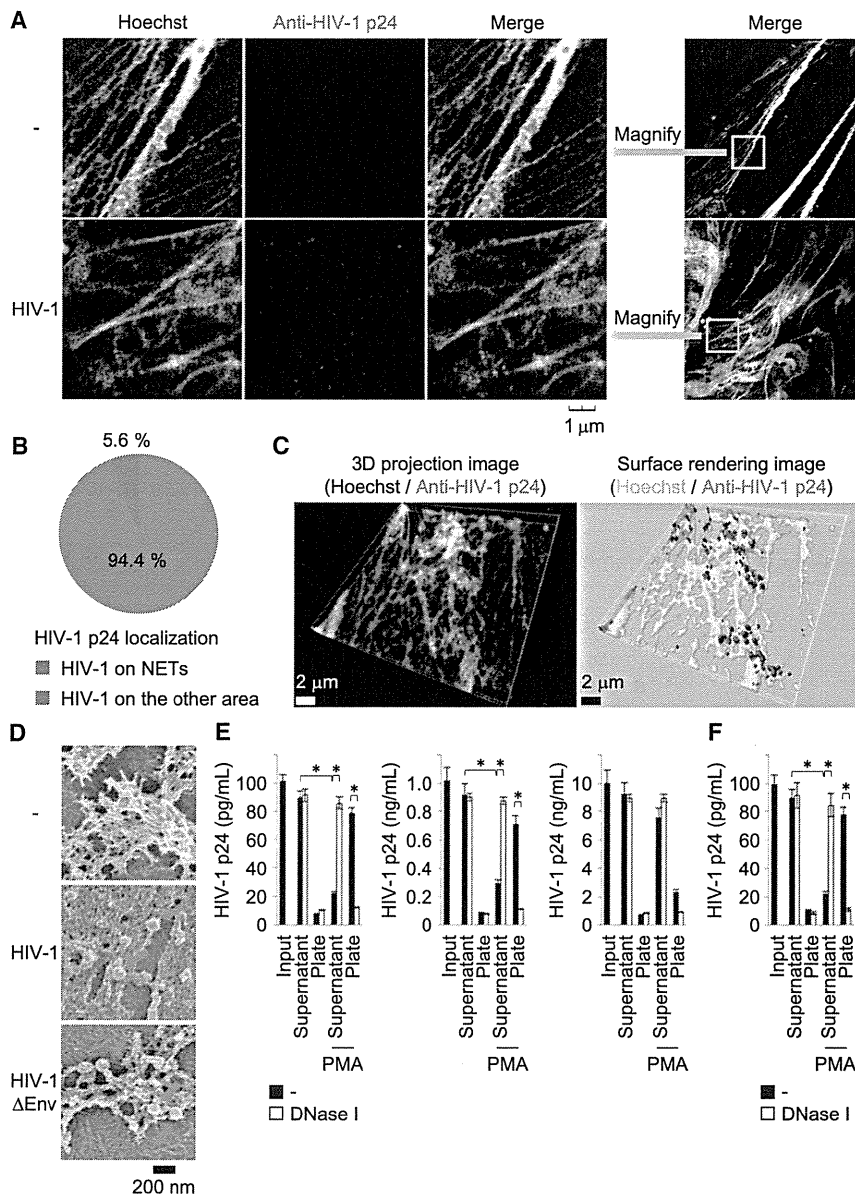


Figure 1. NETs Capture HIV-1

(A–C) Human neutrophils were stimulated with PMA (1 μ M) for 24 hr and were subsequently incubated with or without an HIV-1 vector (p24 antigen, 1.0 ng/mL) for 6 hr. The samples were fixed and subjected to SR-SIM. DNA and HIV-1 virions were detected by Hoechst 33342 and an anti-HIV-1 p24 antibody, respectively (A). The ratio of HIV-1 on NETs was determined (B). A three-dimensional SR-SIM projection image and its surface-rendering image are shown (C). (D) Neutrophils stimulated with PMA were incubated with the HIV-1 vector or the HIV-1 vector lacking the envelope glycoprotein (HIV-1 Δ Env). The samples were fixed and subjected to scanning electron microscopy. The red arrows indicate HIV-1 virions (120 nm spherical structures). (E and F) Neutrophils with or without PMA stimulation were treated with DNase I (50 U/mL) or left untreated for 1 hr. The cells and NETs were then incubated with the indicated dose of HIV-1 vector (E) and HIV-1 Δ Env (F) for 6 hr. The levels of HIV-1 p24 in the culture supernatants and on the culture plates were measured by ELISA. The data shown are means \pm SD (n = 3). Statistical significance (p value) was determined by Student's t test. *p < 0.01. See also Figure S1 and Movie S1.

to the development of acquired immunodeficiency syndrome (AIDS). Thus, elucidation of the antiviral response against HIV-1 is clearly important. Although MPO and α -defensin which are expressed on NETs, have the ability to inactivate HIV-1 (Klebanoff and Coombs, 1992; Moguilevsky et al., 1992; Ding et al., 2009), there are few reports describing a role of NETs in the elimination of HIV-1. Here, we examined the involvement of NETs in the anti-HIV-1 host defense response.

RESULTS

MPO and α -Defensin Inactivate HIV-1 Captured by NETs

Human neutrophils produced NETs consisting of DNA after PMA stimulation (see Figure S1A available online). The size and formation ratio of the NETs were defined by the strength of the PMA stimulation. Superresolution structured illumination

microscopy (SR-SIM), a recently developed imaging technique (Schermelleh et al., 2010), enabled us to observe the structure of the NETs at high resolution, and revealed that the NETs formed multilobulated structures composed of twisted DNA-based fibers (Figure S1B). Scanning electron microscopy (SEM) further confirmed that net-like structures were produced by neutrophils in the extracellular space (Figure S1C).

We used SR-SIM to detect HIV-1 virions, because conventional fluorescence microscopy is unable to detect a single HIV-1 virion with sizes of less than 200 nm, the theoretical resolution limit (Schermelleh et al., 2010). SR-SIM revealed that HIV-1 virions were captured on the outer face and in a ditch of the NETs (Figures 1A–1C). Consistently, SEM revealed that the NETs produced by neutrophils bound to HIV-1 virions as 120 nm spheres (Figure 1D). The HIV-1 Gag protein was detected on the culture plates after stimulation of neutrophils with PMA, but was not detected after DNase I treatment (Figure 1E), indicating that the capture and removal of HIV-1 from the culture supernatant were dependent on DNA on the culture plates. The HIV-1 envelope glycoprotein was not involved in the binding of HIV-1 virions to the NETs (Figures 1D and 1F). A moment of NET binding to HIV-1 virions was observed by the time-lapse imaging analysis (Movie S1). Since histones, major components of NETs, are rich in positively charged basic amino acids, extracellular histones could attract the negatively charged envelope of HIV-1 virions. Consistently, HIV-1 virions were detected on

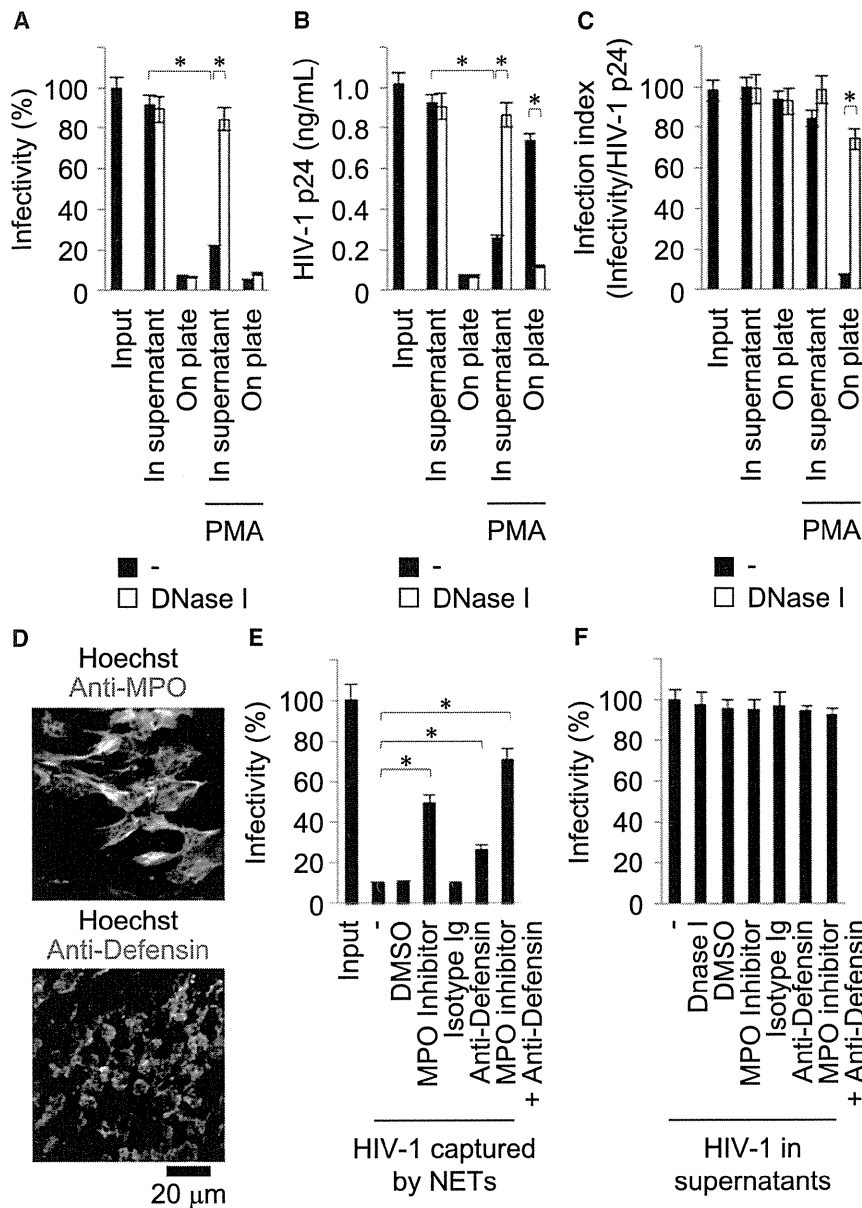


Figure 2. MPO and α -Defensin Mediate NET-Dependent Inactivation of HIV-1

(A–C) Human neutrophils with or without PMA (1 μ M) stimulation were treated with DNase I (50 U/mL) or left untreated for 1 hr. The cells and NETs were then incubated for 6 hr with an HIV-1 vector (p24 antigen, 1.0 ng/mL). The infectivity of the HIV-1 vector in the culture supernatant and on the culture plate was determined (A). The levels of HIV-1 p24 in the culture supernatants and on the culture plates were measured by ELISA (B). A ratio of HIV-1 infectivity per HIV-1 p24 was presented as infection index (arbitrary units) (C). The results shown are means \pm SD (n = 3). Statistical significance (p value) was determined by Student's t test. *p < 0.01.

(D) Neutrophils were stimulated with PMA. The samples were fixed and subjected to immunofluorescence for MPO or α -defensin.

(E) Neutrophils with PMA stimulation were incubated for 6 hr with an HIV-1 vector in the presence of the indicated reagents. After removal of the culture supernatant, the cells and NETs were treated with DNase I for 1 hr to isolate the HIV-1 vector captured by the NETs. The infectivity of the HIV-1 vector on the NETs was determined. The data shown are means \pm SD (n = 3). *p < 0.01. DMSO, dimethyl sulfoxide; Ig, immunoglobulin.

(F) HIV-1 vector was incubated in the presence of the indicated reagents for 6 hr. The infectivity of the HIV-1 vector was determined. The data shown are means \pm SD (n = 3). See also Figure S2.

an antimicrobial activity (Brinkmann et al., 2004), HIV-1 inactivation by NETs was not affected by neutralizing antibody against histone H1 and H2 (data not shown). Histone H3 and H4 might be involved in HIV-1 inactivation by NETs. These findings indicate that NETs ensure high local concentrations of MPO and α -defensin to inactivate HIV-1.

TLR7 and TLR8 Mediate HIV-1 Elimination by NETs

The finding of HIV-1 elimination by NETs prompted us to assess whether the innate

immune system detects HIV-1 and induces NET formation. We found that neutrophils efficiently produced NETs, which were rich in MPO and α -defensin, after stimulation with HIV-1_{MN}, a replication-competent CXCR4-tropic HIV-1 strain (Figure 3A and Figure S2C). Neutrophils also produced NETs after stimulation with the CCR5-tropic strain HIV-1_{JR-FL} and the HIV-1 vector HIV-1_{CSII} (Figure 3A). Neutrophils sensed HIV-1, resulting in the capture of HIV-1 by NETs (Figure 3B). When CD4⁺ T cells and neutrophils were cocultured, neutrophils reduced HIV-1 infection efficiency in an extracellular DNA-dependent manner, indicating that NETs inhibit HIV-1 infection of CD4⁺ T cells (Figure 3C). These findings suggest that pathogen-recognition receptors expressed on neutrophils sense HIV-1 and induce the NET-dependent HIV-1 elimination. Toll-like receptors (TLRs) are the sensors for viruses that induce the antiviral response (Kawai and Akira,

histone H3 of the NETs (Figure S1D). Therefore, NETs capture HIV-1 to prevent HIV-1 from spreading. Next, we assessed whether the infectivity of HIV-1 captured by the NETs was altered. The infectivity of HIV-1 in the culture supernatant was reduced after incubation with PMA-stimulated neutrophils, but was not reduced after DNase I treatment (Figures 2A–2C), indicating that DNA produced by PMA-stimulated neutrophils mediates inactivation of HIV-1. Immunofluorescence analyses revealed that MPO and α -defensin were abundantly expressed on the NETs produced by neutrophils (Figure 2D, Figures S2A and S2B). Inhibition of MPO activity and neutralization of α -defensin resulted in an impaired virucidal response to HIV-1 on the NETs (Figure 2E). However, MPO inhibitor and anti- α -defensin-neutralizing antibody did not directly affect infectivity of HIV-1 (Figure 2F). Although histones have

immune system detects HIV-1 and induces NET formation. We found that neutrophils efficiently produced NETs, which were rich in MPO and α -defensin, after stimulation with HIV-1_{MN}, a replication-competent CXCR4-tropic HIV-1 strain (Figure 3A and Figure S2C). Neutrophils also produced NETs after stimulation with the CCR5-tropic strain HIV-1_{JR-FL} and the HIV-1 vector HIV-1_{CSII} (Figure 3A). Neutrophils sensed HIV-1, resulting in the capture of HIV-1 by NETs (Figure 3B). When CD4⁺ T cells and neutrophils were cocultured, neutrophils reduced HIV-1 infection efficiency in an extracellular DNA-dependent manner, indicating that NETs inhibit HIV-1 infection of CD4⁺ T cells (Figure 3C). These findings suggest that pathogen-recognition receptors expressed on neutrophils sense HIV-1 and induce the NET-dependent HIV-1 elimination. Toll-like receptors (TLRs) are the sensors for viruses that induce the antiviral response (Kawai and Akira,

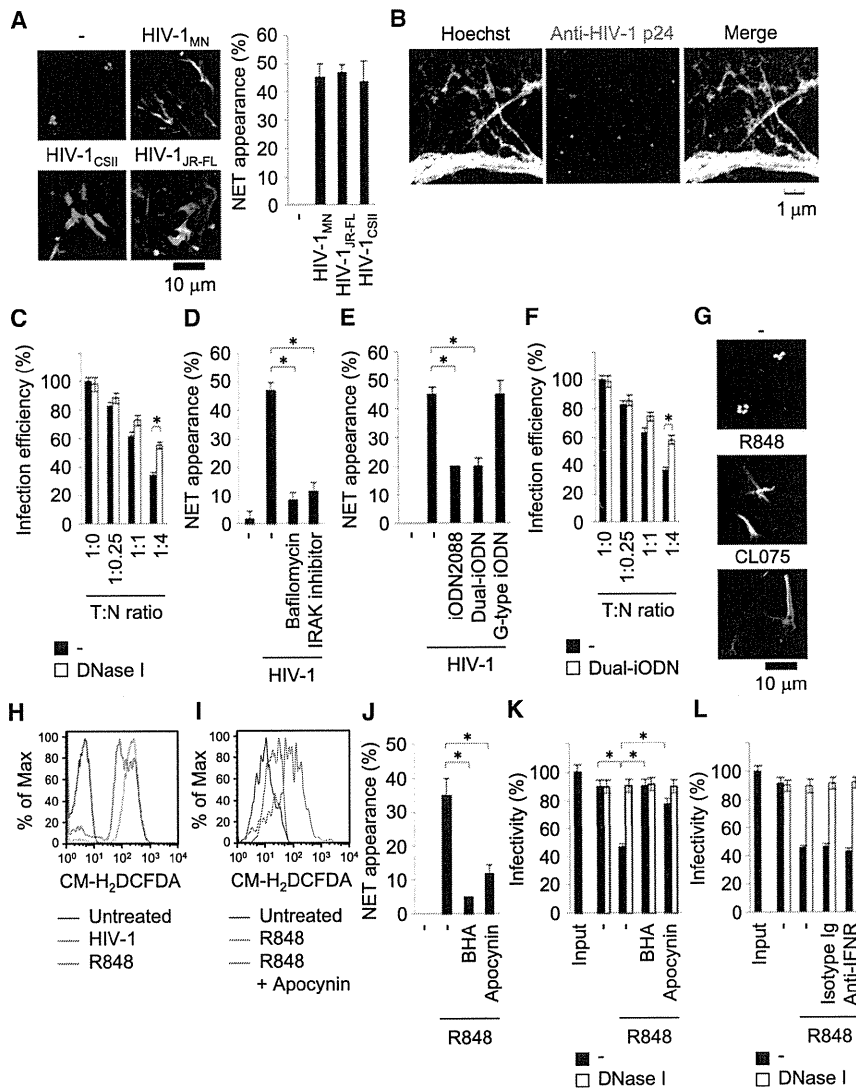


Figure 3. Neutrophils Sense HIV-1 by TLR7 and TLR8 to Produce NETs

(A) Human neutrophils were stimulated for 24 hr with HIV-1_{MN} (p24 antigen, 2.4 ng/mL), HIV-1_{JR-FL} (p24 antigen, 6.0 ng/mL), or HIV-1_{CSII} vector (p24 antigen, 1.0 ng/mL). The samples were fixed and subjected to Hoechst 33342 staining. The rates of NET appearance were measured. The data shown are means \pm SD (n = 3).

(B) Neutrophils were stimulated with HIV-1_{MN} for 24 hr. The samples were fixed and subjected to SR-SIM. DNA and HIV-1 virions were detected by Hoechst 33342 and an anti-HIV-1 p24 antibody, respectively.

(C) CD4⁺ T cells (2 \times 10⁵ cells) were cocultured with neutrophils at the indicated T cell:neutrophil (T:N) ratio. The cells were incubated with an HIV-1 vector in the absence or presence of DNase I (50 U/mL). The efficiency of HIV-1 infection of CD4⁺ T cells was determined. The results shown are means \pm SD (n = 3). Statistical significance (p value) was determined by Student's t test. *p < 0.01.

(D and E) Neutrophils were stimulated for 24 hr with HIV-1_{MN} in the presence of bafilomycin A1 (50 nM) or IRAK inhibitor (1 μ M) (D). Neutrophils were stimulated for 24 hr with HIV-1_{MN} in the presence of iODN2088 (1 μ M), Dual-iODN (1 μ M), or G-type iODN (1 μ M) (E). The rates of NET appearance were measured. The data shown are means \pm SD (n = 3). *p < 0.01.

(F) CD4⁺ T cells were cocultured with neutrophils at the indicated T cell:neutrophil ratio. The cells were incubated with an HIV-1 vector in the absence or presence of Dual-iODN. The efficiency of HIV-1 infection of CD4⁺ T cells was determined. The data shown are means \pm SD (n = 3). *p < 0.01.

(G) Neutrophils were stimulated for 24 hr with R848 (100 nM) or CL075 (500 nM). The samples were fixed and subjected to Hoechst 33342 staining. (H and I) Neutrophils were stimulated with HIV-1 vector for 4 hr or R848 for 2 hr (H). Neutrophils were pretreated with or without apocynin (1 μ M) for 30 min and subsequently stimulated with R848 for 2 hr (I). The cells were then stained with CM-H₂DCFDA (1 μ M). The level of cytoplasmic ROS was measured by FACS.

(J and K) Neutrophils were pretreated with or without BHA (100 μ M) or apocynin for 30 min and subsequently stimulated with R848 for 24 hr. The rates of NET appearance were measured (J). The cells and NETs were then treated with DNase I or left untreated and were subsequently incubated with an HIV-1 vector. The infectivity of the HIV-1 vector in the culture supernatant was determined (K). The data shown are means \pm SD (n = 3). *p < 0.01.

(L) Neutrophils were stimulated with R848 for 24 hr in the presence of anti-type I IFN receptor-neutralizing antibody or control isotype antibody. The cells and NETs were then treated with DNase I or left untreated and were subsequently incubated with an HIV-1 vector. The infectivity of the HIV-1 vector in the culture supernatant was determined. The data shown are means \pm SD (n = 3). See also Figure S3.

2009). In particular, TLR7 and TLR8 detect single-stranded RNA of the HIV-1 genome on plasmacytoid dendritic cells to induce the production of type I interferon, cytokines, and chemokines (Beignon et al., 2005; Heil et al., 2004; Gringhuis et al., 2010). Because multiple TLRs are expressed on neutrophils and mediate ROS production (Hayashi et al., 2003; Hoarau et al., 2007; Wang et al., 2008), we examined an involvement of the TLR family members in NET formation induced by HIV-1. Inhibition of the vacuolar type H⁺-ATPase by bafilomycin A1 resulted in the suppression of HIV-1-induced NET formation (Figure 3D), suggesting that endolysosomal TLRs such as TLR3, TLR7, TLR8, and TLR9 mediate NET formation. Chemical inhibition of

interleukin-1 receptor-associated kinase 4 (IRAK4), a critical regulator of all TLRs except TLR3 (Kawai and Akira, 2009), also resulted in the suppression of HIV-1-induced NET formation (Figure 3D), suggesting that TLR7, TLR8, and TLR9 are involved in NET formation. Neither bafilomycin A1 nor the IRAK4 inhibitor suppressed NET formation by PMA, and these compounds did not affect cell viability (Figures S3A and S3B). Dual-iODN and iODN2088, antagonists for TLR7, TLR8, and TLR9, inhibited NET formation by HIV-1, whereas G-type iODN, a selective antagonist for TLR9, did not alter NET formation efficiency (Figure 3E). These inhibitory oligonucleotides did not affect NET formation by PMA and cell viability (Figures S3C and S3D).

When CD4⁺ T cells and neutrophils were cocultured, neutrophils reduced HIV-1 infection efficiency in a TLR7- and TLR8-dependent manner (Figure 3F). These findings indicate that TLR7 and TLR8 are responsible for the NET-dependent HIV-1 elimination.

We next examined the molecular mechanism of TLR7- and TLR8-mediated NET formation. We focused on a role of ROS, because NADPH oxidase-dependent ROS generation was involved in the NET-dependent elimination of HIV-1 by PMA (Figures S3E–S3G). Neutrophils produced NETs, which were rich in MPO and α -defensin, in response to R848 and CL075, synthetic ligands for TLR7 and TLR8 (Figure 3G and Figure S2D). Both HIV-1 and R848 triggered the generation of ROS, and R848-induced ROS generation was mediated by NADPH oxidase (Figures 3H and 3I). Butylated hydroxyanisole (BHA), a ROS scavenger, and apocynin, an inhibitor of NADPH oxidase, inhibited the NET formation induced by R848, but did not alter cell viability (Figure 3J and Figure S3H). Consistently, R848 induced NET-dependent HIV-1 elimination through ROS generated by NADPH oxidase (Figure 3K). Type I IFN, which is often slightly induced by R848 (Kawai and Akira, 2009), was not involved in NET-dependent HIV-1 elimination (Figure 3L). Thus, TLR7 and TLR8 induce NADPH oxidase-dependent ROS generation to eliminate HIV-1 by NETs.

HIV-1 Induces CD209-Dependent IL-10 Production by Dendritic Cells to Escape the NET-Dependent Antiviral Response

Accumulating evidence has revealed that HIV-1 evolves to manage immune cells, especially dendritic cells, for its efficient propagation. For example, HIV-1 binds to the dendritic cell-specific lectin CD209, also called DC-SIGN, to move along an infectious synapse generated between CD209⁺ dendritic cells and CD4⁺ T cells, resulting in efficient infection of CD4⁺ T cells (Geijtenbeek et al., 2000; Arrighi et al., 2004). Since mucosal tissues are rich in CD209⁺ dendritic cells and CD4⁺ T cells, HIV-1 uses these tissues as major HIV-1 entry routes (Geijtenbeek et al., 2000; Jameson et al., 2002). Importantly, mucosal tissues are also rich in neutrophils, and NETs are suggested to be involved in the mucosal inflammation (Mumy and McCormick, 2009; Savchenko et al., 2011). Therefore, we assessed whether HIV-1 makes use of CD209⁺ dendritic cells to escape the NET-dependent antiviral response. Neutrophils produced NETs less efficiently in response to R848 after exposure to the culture supernatant of monocyte-derived dendritic cells incubated with HIV-1 (Figure 4A). HIV-1 with the envelope glycoprotein, but not HIV-1 lacking the envelope glycoprotein, induced the production of a NET-suppressive factor by dendritic cells (Figure 4A). Consistently, recombinant gp120 induced the production of the NET-suppressive factor by dendritic cells (Figure 4A). CD4, CXCR4, and CD209 are known to bind to the envelope glycoprotein of CXCR4-tropic HIV-1 and to induce an immune response (Lee et al., 2003; Shan et al., 2007). An anti-CD209-neutralizing antibody inhibited the production of the NET-suppressive factor by dendritic cells stimulated with HIV-1, but did not alter viability of dendritic cells and neutrophils (Figures 4B and 4C), indicating that HIV-1 stimulated CD209 on dendritic cells to suppress TLR-mediated NET formation. However, neither an anti-CD4-neutralizing antibody nor the CXCR4 antagonist T22 affected the production of the NET-suppressive factor

by dendritic cells incubated with HIV-1 (Figure 4B). Thus, HIV-1 takes advantage of the functions of CD209 on dendritic cells not only for efficient infection of the target cells but also to escape the NET-mediated antiviral system.

Previous studies have revealed that the immunosuppressive cytokine interleukin (IL)-10 is produced by dendritic cells after engagement of CD209, and that the expression level of plasma IL-10 correlates with the progression of AIDS (Stylianou et al., 1999; Geijtenbeek et al., 2003; Shan et al., 2007; Naicker et al., 2009). IL-33 is also produced by dendritic cells after engagement of CD209 and suppresses inflammation through a unique T_H2 pathway (Anthony et al., 2011). Next, we attempted to identify the NET-suppressive factor produced by dendritic cells with CD209 stimulation. An anti-IL-10-neutralizing antibody, but not an anti-IL-33-neutralizing antibody, inhibited the suppression of NET formation by the culture supernatant of dendritic cells with CD209 stimulation (Figures 4D and 4E). When CD209⁺ dendritic cells and neutrophils were cocultured, dendritic cells inhibited HIV-1-induced NET formation in a CD209- and IL-10-dependent manner (Figure 4F), strongly suggesting that HIV-1 escapes from NETs under physiological conditions. Consistently, dendritic cells produced IL-10 after sensing HIV-1 with the envelope glycoprotein, but not HIV-1 lacking the envelope glycoprotein (Figures 4G and 4H). Dendritic cells also produced IL-10 after stimulation with recombinant gp120 (Figure 4H), indicating that CD209 senses HIV-1 envelope glycoprotein to induce IL-10 production. IL-10 inhibited the NET formation and NET-dependent HIV-1 elimination induced by R848, but did not alter cell viability (Figures 4I and 4J and Figure S3I). However, IL-10 failed to inhibit the NET formation and HIV-1 elimination induced by PMA (Figures S3J and S3K). Therefore, HIV-1 induces CD209-dependent production of IL-10 by dendritic cells to suppress NET formation.

IL-10 is known to suppress the inflammatory immune response by blocking activation of the TLR signaling pathway (Chang et al., 2009). Phosphorylation of NCF1 is a key step in activation of the NADPH oxidase complex (Johnson et al., 1998; Dang et al., 2006). IL-10 inhibited R848-induced assembly of p38 MAPK and NCF1 (Figure S4A) and phosphorylation of NCF1 (Figure 4K). Consistently, IL-10 inhibited R848-induced generation of ROS and subsequent nuclear translocation of neutrophil elastase (Figure 4L and Figure S4B). However IL-10 did not inhibit NADPH oxidase-dependent ROS generation and nuclear translocation of neutrophil elastase induced by PMA (Figures S3L, S4A, and S4B). These findings indicated that IL-10 inhibits TLR7- and TLR8-signaling pathway, resulting in the suppression of NADPH oxidase-dependent NET formation.

DISCUSSION

In the present study, we have shown NET induction by the innate immune system and HIV-1 elimination by NETs. Previous studies have revealed that NETs also eliminate *Staphylococcus aureus* and *Candida albicans*, causative agents of opportunistic infections in AIDS patients (Haseltine, 1988; Brinkmann et al., 2004; Urban et al., 2009). Thus, induction of NET formation seems to be a promising immunotherapeutic strategy for AIDS patients. However, there are difficulties associated with eliminating HIV-1 by NETs. This is because a progressive decrease in the

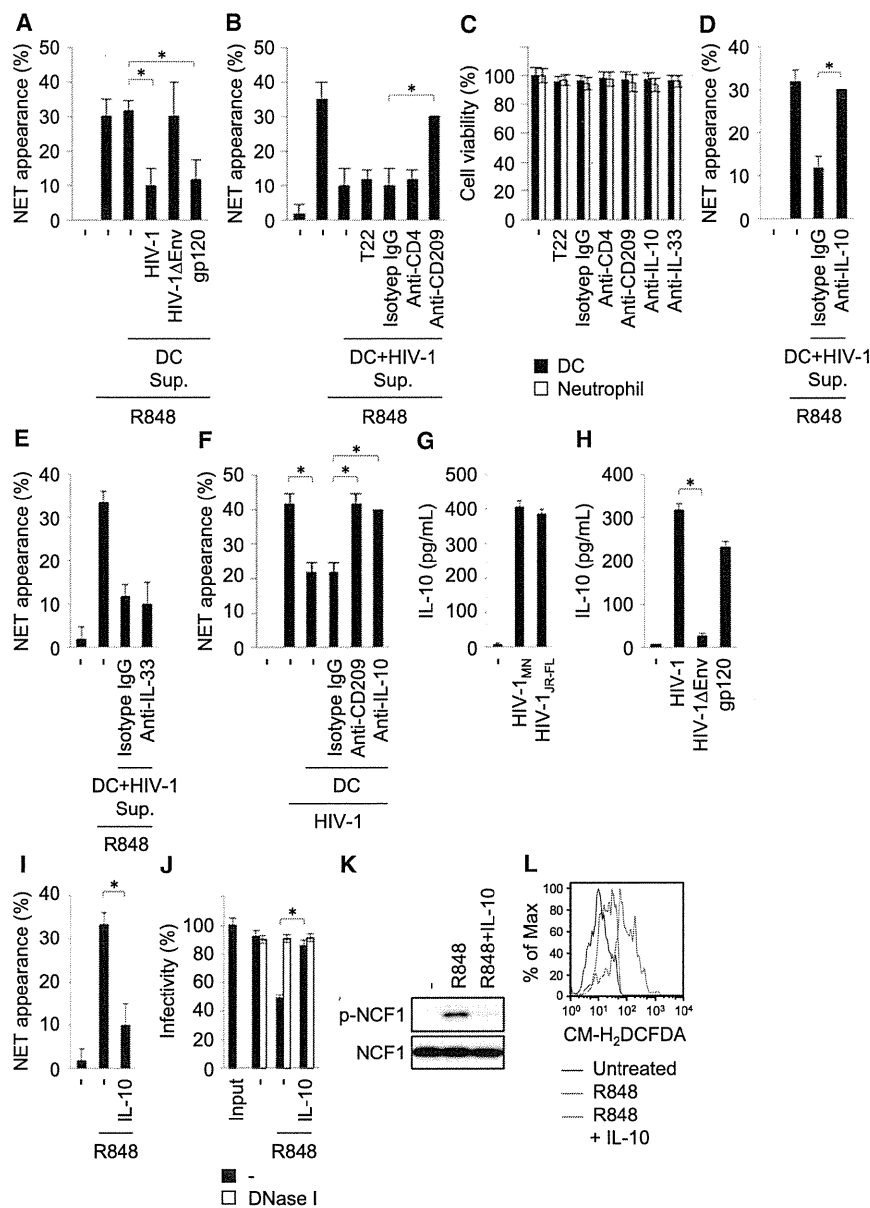


Figure 4. HIV-1 Causes CD209-Dependent IL-10 Production by Dendritic Cells to Suppress NET Formation

(A) Human monocyte-derived dendritic cells (2×10^5 cells) were stimulated with or without HIV-1 vector (p24 antigen, 1.0 ng/mL), HIV-1ΔEnv, or gp120 (1.0 μg/mL) for 24 hr. Seven days later, autologous neutrophils (2×10^5 cells) were isolated and treated with or without the indicated culture supernatant of dendritic cells for 6 hr. The cells were subsequently stimulated with or without R848 (100 nM) for 24 hr. The rates of NET appearance were measured. The results shown are means \pm SD ($n = 3$). Statistical significance (p value) was determined by Student's t test. * $p < 0.01$. DC, dendritic cells; Sup., culture supernatant.

(B) Dendritic cells were stimulated with HIV-1 vector for 24 hr in the presence of the CXCR4 antagonist T22, CD4-neutralizing antibody, CD209-neutralizing antibody, or control isotype antibody. Autologous neutrophils were pretreated with or without the indicated culture supernatant of dendritic cells for 6 hr and subsequently stimulated with or without R848 for 24 hr. The rates of NET appearance were measured. The data shown are means \pm SD ($n = 3$). * $p < 0.01$.

(C) Dendritic cells and neutrophils were cultured in the presence of indicated reagents for 24 hr. The cell viability was measured by CellTiter-Glo kit. The data shown are means \pm SD ($n = 3$).

(D and E) Dendritic cells were stimulated with HIV-1 vector for 24 hr. Autologous neutrophils were pretreated for 6 hr with or without the culture supernatant of HIV-1-stimulated dendritic cells in the presence of anti-IL-10-neutralizing antibody (D), anti-IL-33-neutralizing antibody (E), or control isotype antibody. The neutrophils were subsequently stimulated with or without R848 for 24 hr. The rates of NET appearance were measured. The data shown are means \pm SD ($n = 3$). * $p < 0.01$.

(F) Neutrophils and dendritic cells were stimulated with HIV-1 vector for 24 hr in the presence of CD209-neutralizing antibody, IL-10-neutralizing antibody, or control isotype antibody. The rates of NET appearance were measured. The data shown are means \pm SD ($n = 3$). * $p < 0.01$.

(G and H) Dendritic cells were stimulated for 24 hr with or without HIV-1_{MN} or HIV-1_{JR-FL} (G). Dendritic

cells were stimulated for 24 hr with or without HIV-1 vector, HIV-1ΔEnv, or gp120 (H). The levels of IL-10 in the culture supernatants were measured by ELISA. The data shown are means \pm SD ($n = 3$). * $p < 0.01$.

(I and J) Neutrophils were pretreated with or without IL-10 (10 ng/mL) for 6 hr and subsequently stimulated with R848 for 24 hr. The rates of NET appearance were measured (I). The cells and NETs were then treated with DNase I (50 U/mL) or left untreated, and subsequently incubated with an HIV-1 vector. The infectivity of the HIV-1 vector in the culture supernatant was determined (J). The data shown are means \pm SD ($n = 3$). * $p < 0.01$.

(K) Neutrophils were pretreated with or without IL-10 for 6 hr and subsequently stimulated with R848 for 1 hr. The cell lysates were subjected to immunoblotting with antibodies against the indicated proteins.

(L) Neutrophils were pretreated with or without IL-10 for 6 hr and subsequently stimulated with R848 for 2 hr. The cells were then stained with CM-H₂DCFDA (1 μM). The level of cytoplasmic ROS was measured by FACS. See also Figure S4.

number of neutrophils occurs in AIDS patients, and the host defense systems are disrupted by HIV-1 (Scadden, 1992; Shan et al., 2007; D'Souza et al., 2008). The severe neutropenia and immune disruption by HIV-1 might complicate HIV-1 elimination by the NET antiviral system and lead to the progression of AIDS. To recover well from neutropenia, administration of granulocyte monocyte colony-stimulating factor (GM-CSF) or granulocyte

colony-stimulating factor (G-CSF) is effective (Scadden, 1992; D'Souza et al., 2008). These growth factors stimulate the survival, proliferation, differentiation, and function of neutrophil precursors and mature neutrophils. In addition, GM-CSF has the ability to assist NET formation (Martinelli et al., 2004). Inhibition of HIV-1 interactions with CD209 may also support induction of the NET antiviral system because IL-10 inhibits not only the

formation of NETs but also the activation of the G-CSF and GM-CSF signaling pathways (Dang et al., 2006; Yoshimura et al., 2007). Therefore, a combination therapy, with recovery from neutropenia and inhibition of HIV-1 immune escape, may be effective in AIDS patients.

EXPERIMENTAL PROCEDURES

Titration of HIV-1

Neutrophils (2×10^5 cells) were treated as indicated and then incubated for 6 hr with an HIV-1 vector capable of expressing firefly luciferase after integration into the host genome. Alternatively, the HIV-1 vector incubated for 6 hr in the absence of neutrophils was used as input control. Molt-4 T cells (2×10^5 cells) were incubated with the culture supernatant for 48 hr to determine the infectivity of the HIV-1 vector in the culture supernatant. Separately, Molt-4 T cells were seeded into a culture plate after harvesting of the culture supernatant and were incubated for 48 hr to determine the infectivity of the HIV-1 vector on the culture plate. After the incubation, the Molt-4 T cells were subjected to a luciferase reporter assay. The luciferase activity in Molt-4 T cells infected with the treated HIV-1 vector was divided by the luciferase activity in Molt-4 T cells infected with the input HIV-1 vector to determine the infectivity of the treated HIV-1 vector. The experiments were performed in accordance with the guidelines of the ethics committee of Osaka University.

Immunocytochemistry

Immunofluorescence staining was performed as previously described (Saitoh et al., 2011). The samples were examined under an IX81-DSU spinning disc confocal microscope (Olympus). For measurement of the efficiency of NET formation, 20 fields of view in each sample (each $100 \times 100 \mu\text{m}$) were randomly chosen for analysis. The number of views with NETs was counted to measure the rate of NET appearance.

Superresolution images of the samples were obtained using an Elyra SR-SIM (Zeiss). For measurement of the efficiency of HIV-1 capture by NETs, six fields of view in each sample (each $5 \times 5 \mu\text{m}$) were randomly chosen for analysis. Rendering of z stack SR-SIM images by the software Imapris (Bitplane AG) was used to construct the three-dimensional SR-SIM image.

SEM Analysis

Samples on plastic coverslips were fixed with 2% formaldehyde and 2.5% glutaraldehyde in 0.1 M cacodylate buffer (pH 7.4), postfixed with 1% osmium tetroxide and 0.5% potassium ferrocyanide in the same buffer, dehydrated through a graded series of ethanol, substituted with t-butyl alcohol, and freeze-dried. After freeze-drying, the samples were coated with osmium tetroxide and observed with a S-4800 field emission scanning electron microscope (Hitachi High-Technologies).

Immunoblotting

Immunoblotting was performed as previously described (Saitoh et al., 2011).

ELISA

The levels of HIV-1 p24 and IL-10 were measured by ELISA according to the manufacturer's instructions.

Fluorescence-Activated Cell Sorting

Fluorescence-activated cell sorting (FACS) was performed as previously described (Saitoh et al., 2011).

SUPPLEMENTAL INFORMATION

Supplemental Information includes four figures, one movie, Supplemental Experimental Procedures, and Supplemental References and can be found with this article online at <http://dx.doi.org/10.1016/j.chom.2012.05.015>.

ACKNOWLEDGMENTS

We are grateful to Drs. D. Trono, H. Miyoshi, G. Melikian, and Y. Koyanagi for providing invaluable materials. We also thank the members of the Laboratory

of Host Defense for their assistance. This work was supported by JSPS KAKENHI Grant Number 23659231 (to T.S.), JSPS KAKENHI Grant Number 20002008 (to S.A.), JSPS Funding Program for World-Leading Innovative R&D on Science and Technology (to S.A.), and National Institutes of Health Grant P01 AI070167 (to S.A.).

Received: September 7, 2011

Revised: January 27, 2012

Accepted: May 18, 2012

Published: July 18, 2012

REFERENCES

- Anthony, R.M., Kobayashi, T., Wermeling, F., and Ravetch, J.V. (2011). Intravenous gammaglobulin suppresses inflammation through a novel T(H)2 pathway. *Nature* *475*, 110–113.
- Arrighi, J.F., Pion, M., Garcia, E., Escola, J.M., van Kooyk, Y., Geijtenbeek, T.B., and Piguet, V. (2004). DC-SIGN-mediated infectious synapse formation enhances X4 HIV-1 transmission from dendritic cells to T cells. *J. Exp. Med.* *200*, 1279–1288.
- Beignon, A.S., McKenna, K., Skoberne, M., Manches, O., DaSilva, I., Kavanagh, D.G., Larsson, M., Gorelick, R.J., Lifson, J.D., and Bhardwaj, N. (2005). Endocytosis of HIV-1 activates plasmacytoid dendritic cells via Toll-like receptor-viral RNA interactions. *J. Clin. Invest.* *115*, 3265–3275.
- Brinkmann, V., Reichard, U., Goosmann, C., Fauler, B., Uhlemann, Y., Weiss, D.S., Weinrauch, Y., and Zychlinsky, A. (2004). Neutrophil extracellular traps kill bacteria. *Science* *303*, 1532–1535.
- Chang, J., Kunkel, S.L., and Chang, C.H. (2009). Negative regulation of MyD88-dependent signaling by IL-10 in dendritic cells. *Proc. Natl. Acad. Sci. USA* *106*, 18327–18332.
- Dang, P.M., Elbim, C., Marie, J.C., Chiandotto, M., Gougerot-Pocidal, M.A., and El-Benna, J. (2006). Anti-inflammatory effect of interleukin-10 on human neutrophil respiratory burst involves inhibition of GM-CSF-induced p47PHOX phosphorylation through a decrease in ERK1/2 activity. *FASEB J.* *20*, 1504–1506.
- Ding, J., Chou, Y.Y., and Chang, T.L. (2009). Defensins in viral infections. *J. Innate Immun.* *1*, 413–420.
- D'Souza, A., Jaiyesimi, I., Trainor, L., and Venuturumili, P. (2008). Granulocyte colony-stimulating factor administration: adverse events. *Transfus. Med. Rev.* *22*, 280–290.
- Fuchs, T.A., Abed, U., Goosmann, C., Hurwitz, R., Schulze, I., Wahn, V., Weinrauch, Y., Brinkmann, V., and Zychlinsky, A. (2007). Novel cell death program leads to neutrophil extracellular traps. *J. Cell Biol.* *176*, 231–241.
- Geijtenbeek, T.B., Kwon, D.S., Torensma, R., van Vliet, S.J., van Duijnhoven, G.C., Middel, J., Cornelissen, I.L., Nottet, H.S., KewalRamani, V.N., Littman, D.R., et al. (2000). DC-SIGN, a dendritic cell-specific HIV-1-binding protein that enhances trans-infection of T cells. *Cell* *100*, 587–597.
- Geijtenbeek, T.B., Van Vliet, S.J., Koppel, E.A., Sanchez-Hernandez, M., Vandembroucke-Grauls, C.M., Appelmelk, B., and Van Kooyk, Y. (2003). Mycobacteria target DC-SIGN to suppress dendritic cell function. *J. Exp. Med.* *197*, 7–17.
- Gringhuis, S.I., van der Vlist, M., van den Berg, L.M., den Dunnen, J., Litjens, M., and Geijtenbeek, T.B. (2010). HIV-1 exploits innate signaling by TLR8 and DC-SIGN for productive infection of dendritic cells. *Nat. Immunol.* *11*, 419–426.
- Hakkim, A., Fuchs, T.A., Martinez, N.E., Hess, S., Prinz, H., Zychlinsky, A., and Waldmann, H. (2011). Activation of the Raf-MEK-ERK pathway is required for neutrophil extracellular trap formation. *Nat. Chem. Biol.* *7*, 75–77.
- Haseltine, W.A. (1988). Replication and pathogenesis of the AIDS virus. *J. Acquir. Immune Defic. Syndr.* *1*, 217–240.
- Hayashi, F., Means, T.K., and Luster, A.D. (2003). *Blood* *102*, 2660–2669.
- Heil, F., Hemmi, H., Hochrein, H., Ampenberger, F., Kirschning, C., Akira, S., Lipford, G., Wagner, H., and Bauer, S. (2004). Species-specific recognition of single-stranded RNA via toll-like receptor 7 and 8. *Science* *303*, 1526–1529.

- Hemmers, S., Teijaro, J.R., Arandjelovic, S., and Mowen, K.A. (2011). PAD4-mediated neutrophil extracellular trap formation is not required for immunity against influenza infection. *PLoS ONE* 6, e22043. <http://dx.doi.org/10.1371/journal.pone.0022043>.
- Hoarau, C., Gérard, B., Lescanne, E., Henry, D., François, S., Lacapère, J.J., El Benna, J., Dang, P.M., Grandchamp, B., Lebranchu, Y., et al. (2007). TLR9 activation induces normal neutrophil responses in a child with IRAK-4 deficiency: involvement of the direct PI3K pathway. *J. Immunol.* 179, 4754–4765.
- Jameson, B., Baribaud, F., Pöhlmann, S., Ghavimi, D., Mortari, F., Doms, R.W., and Iwasaki, A. (2002). Expression of DC-SIGN by dendritic cells of intestinal and genital mucosae in humans and rhesus macaques. *J. Virol.* 76, 1866–1875.
- Johnson, J.L., Park, J.W., Benna, J.E., Faust, L.P., Inanami, O., and Babior, B.M. (1998). Activation of p47(PHOX), a cytosolic subunit of the leukocyte NADPH oxidase. Phosphorylation of ser-359 or ser-370 precedes phosphorylation at other sites and is required for activity. *J. Biol. Chem.* 273, 35147–35152.
- Kawai, T., and Akira, S. (2009). The roles of TLRs, RLRs and NLRs in pathogen recognition. *Int. Immunol.* 21, 317–337.
- Kiebanoff, S.J., and Coombs, R.W. (1992). Viricidal effect of polymorphonuclear leukocytes on human immunodeficiency virus-1. Role of the myeloperoxidase system. *J. Clin. Invest.* 89, 2014–2017.
- Lee, C., Liu, Q.H., Tomkowicz, B., Yi, Y., Freedman, B.D., and Collman, R.G. (2003). Macrophage activation through CCR5- and CXCR4-mediated gp120-elicited signaling pathways. *J. Leukoc. Biol.* 74, 676–682.
- Martinelli, S., Urosevic, M., Daryadel, A., Oberholzer, P.A., Baumann, C., Fey, M.F., Dummer, R., Simon, H.U., and Yousefi, S. (2004). Induction of genes mediating interferon-dependent extracellular trap formation during neutrophil differentiation. *J. Biol. Chem.* 279, 44123–44132.
- Moguilevsky, N., Steens, M., Thiriart, C., Prieels, J.P., Thiry, L., and Bollen, A. (1992). Lethal oxidative damage to human immunodeficiency virus by human recombinant myeloperoxidase. *FEBS Lett.* 302, 209–212.
- Mumy, K.L., and McCormick, B.A. (2009). The role of neutrophils in the event of intestinal inflammation. *Curr. Opin. Pharmacol.* 9, 697–701.
- Naicker, D.D., Werner, L., Kormuth, E., Passmore, J.A., Mlisana, K., Karim, S.A., and Ndung'u, T. (2009). Interleukin-10 promoter polymorphisms influence HIV-1 susceptibility and primary HIV-1 pathogenesis. *J. Infect. Dis.* 200, 448–452.
- Narasaraju, T., Yang, E., Samy, R.P., Ng, H.H., Poh, W.P., Liew, A.A., Phoon, M.C., van Rooijen, N., and Chow, V.T. (2011). Excessive neutrophils and neutrophil extracellular traps contribute to acute lung injury of influenza pneumonia. *Am. J. Pathol.* 179, 199–210.
- Papayannopoulos, V., and Zychlinsky, A. (2009). NETs: a new strategy for using old weapons. *Trends Immunol.* 30, 513–521.
- Papayannopoulos, V., Metzler, K.D., Hakkim, A., and Zychlinsky, A. (2010). Neutrophil elastase and myeloperoxidase regulate the formation of neutrophil extracellular traps. *J. Cell Biol.* 191, 677–691.
- Saitoh, T., Satoh, T., Yamamoto, N., Uematsu, S., Takeuchi, O., Kawai, T., and Akira, S. (2011). Antiviral protein Viperin promotes Toll-like receptor 7- and Toll-like receptor 9-mediated type I interferon production in plasmacytoid dendritic cells. *Immunity* 34, 352–363.
- Savchenko, A.S., Inoue, A., Ohashi, R., Jiang, S., Hasegawa, G., Tanaka, T., Hamakubo, T., Kodama, T., Aoyagi, Y., Ushiki, T., et al. (2011). Long pentraxin 3 (PTX3) expression and release by neutrophils in vitro and in ulcerative colitis. *Pathol. Int.* 61, 290–297.
- Scadden, D.T. (1992). The use of GM-CSF in AIDS. *Infection* 20 (Suppl. 2), S103–S106.
- Schermelleh, L., Heintzmann, R., and Leonhardt, H. (2010). A guide to super-resolution fluorescence microscopy. *J. Cell Biol.* 190, 165–175.
- Shan, M., Klasse, P.J., Banerjee, K., Dey, A.K., Iyer, S.P., Dionisio, R., Charles, D., Campbell-Gardener, L., Olson, W.C., Sanders, R.W., et al. (2007). HIV-1 gp120 mannoses induce immunosuppressive responses from dendritic cells. *PLoS Pathog.* 3, e169.
- Stylianou, E., Aukrust, P., Kvale, D., Müller, F., and Frøland, S.S. (1999). IL-10 in HIV infection: increasing serum IL-10 levels with disease progression—down-regulatory effect of potent anti-retroviral therapy. *Clin. Exp. Immunol.* 116, 115–120.
- Urban, C.F., Ermert, D., Schmid, M., Abu-Abed, U., Goosmann, C., Nacken, W., Brinkmann, V., Jungblut, P.R., and Zychlinsky, A. (2009). Neutrophil extracellular traps contain calprotectin, a cytosolic protein complex involved in host defense against *Candida albicans*. *PLoS Pathog.* 5, e1000639. <http://dx.doi.org/10.1371/journal.ppat.1000639>.
- von Köckritz-Blickwedde, M., Goldmann, O., Thulin, P., Heinemann, K., Norrby-Teglund, A., Rohde, M., and Medina, E. (2008). Phagocytosis-independent antimicrobial activity of mast cells by means of extracellular trap formation. *Blood* 111, 3070–3080.
- Wang, J.P., Bowen, G.N., Padden, C., Cerny, A., Finberg, R.W., Newburger, P.E., and Kurt-Jones, E.A. (2008). Toll-like receptor-mediated activation of neutrophils by influenza A virus. *Blood* 112, 2028–2034.
- Wardini, A.B., Guimarães-Costa, A.B., Nascimento, M.T., Nadaes, N.R., Danelli, M.G., Mazur, C., Benjamim, C.F., Saraiva, E.M., and Pinto-da-Silva, L.H. (2010). Characterization of neutrophil extracellular traps in cats naturally infected with feline leukemia virus. *J. Gen. Virol.* 91, 259–264.
- Yoshimura, A., Naka, T., and Kubo, M. (2007). SOCS proteins, cytokine signaling and immune regulation. *Nat. Rev. Immunol.* 7, 454–465.
- Yousefi, S., Gold, J.A., Andina, N., Lee, J.J., Kelly, A.M., Kozłowski, E., Schmid, I., Straumann, A., Reichenbach, J., Gleich, G.J., et al. (2008). Catapult-like release of mitochondrial DNA by eosinophils contributes to antibacterial defense. *Nat. Med.* 14, 949–953.
- Yousefi, S., Mihalache, C., Kozłowski, E., Schmid, I., and Simon, H.U. (2009). Viable neutrophils release mitochondrial DNA to form neutrophil extracellular traps. *Cell Death Differ.* 16, 1438–1444.

Structural Modulation Study of Inhibitory Compounds for Ribonuclease H Activity of Human Immunodeficiency Virus Type 1 Reverse Transcriptase

Hiroshi Yanagita,^a Satoshi Fudo,^a Emiko Urano,^b Reiko Ichikawa,^b Masakazu Ogata,^a Mizuho Yokota,^a Tsutomu Murakami,^b Honggui Wu,^{b,c} Joe Chiba,^c Jun Komano,^b and Tyuji Hoshino^{*a}

^aGraduate School of Pharmaceutical Sciences, Chiba University; 1–8–1 Inohana, Chuo-ku, Chiba 260–8675, Japan:

^bAIDS Research Center, National Institute of Infectious Diseases; 1–23–1 Toyama, Shinjuku-ku, Tokyo 162–8640,

Japan; and ^cFaculty of Industrial Science and Technology, Tokyo University of Science; 2641 Yamazaki, Noda, Chiba 278–8510, Japan. Received February 23, 2012; accepted April 4, 2012

Reverse transcriptase of human immunodeficiency virus type 1 (HIV-1) has two enzymatic functions. One of the functions is ribonuclease (RNase) H activity concerning the digestion of only RNA of RNA/DNA hybrid. The RNase H activity is an attractive target for a new class of anti-HIV drugs because no approved inhibitor is available now. In our previous studies, an agent bearing 5-nitro-furan-2-carboxylic acid ester core was found from chemical screening and dozens of the derivatives were synthesized to improve compound potency. In this work, some parts of the chemical structure were modulated to deepen our understanding of the structure–activity relationship of the analogous compounds. Several derivatives having nitro-furan-phenyl-ester skeleton were shown to be potent RNase H inhibitors. Attaching methoxy-carbonyl and methoxy groups to the phenyl ring increased the inhibitory potency. No significant cytotoxicity was observed for these active derivatives. In contrast, the derivatives having nitro-furan-benzyl-ester skeleton showed modest inhibitory activities regardless of attaching diverse kinds of functional groups to the benzyl ring. Both the modulation of the 5-nitro-furan-2-carboxylic moiety and the conversion of the ester linkage resulted in a drastic decrease in inhibitory potency. These findings are informative for designing potent inhibitors of RNase H enzymatic activity of HIV-1.

Key words antiviral drug; ribonuclease H enzymatic activity; nitro-furan-phenyl-ester; human immunodeficiency virus type 1 reverse transcriptase; inhibitor

Human immunodeficiency virus type 1 (HIV-1) reverse transcriptase (RT) is a multi-functional enzyme that facilitates both polymerase and ribonuclease (RNase) H activities and converts the single-stranded viral RNA into a double-stranded DNA. There exist two active sites in HIV-1 RT responsible for the respective enzymatic functions. Currently, two classes of RT inhibitors, nucleoside reverse transcriptase inhibitors (NRTIs) and non-nucleoside reverse transcriptase inhibitors (NNRTIs), are used clinically. The formers compete with the natural deoxyribonucleotide triphosphate (dNTP) for nucleoside incorporation and act as chain terminators after incorporation.¹⁾ The latter agents are bound to an adjacent location from the polymerase active site and block RT polymerase function.²⁾ Both of these inhibitors are targeting polymerase activity of RT. In contrast, no approved inhibitor is available for RNase H activity, although there have been several reports on the inhibitors that target the RNase H activity of HIV-1 RT.^{3–5)} The role of RNase H activity in the reverse transcription process is to remove the viral genomic RNA during the synthesis of double-stranded DNA.^{6,7)} Agents targeting RNase H function is expected to be complimentary to the currently standard chemotherapy. Hence, RT-associated RNase H activity is one of the attractive targets for developing a novel class of antiviral drugs. Furthermore, the potential for dual inhibition of RNase H activity and integrase activity of HIV-1 has been examined because of the structural similarity of their catalytic sites.^{8–10)}

HIV-1 RNase H is known to utilize two divalent metals

for catalysis.^{11–13)} The RNase H dual metal mechanism was suggested from high resolution co-crystal structures of *Bacillus halodurans* RNase H with RNA/DNA hybrids at different stages along the reaction pathway of phosphodiester cleavage.^{14,15)} The active site contains four carboxyl residues, creating an environment capable of holding two metal ions. It has been assumed that many RNase H inhibitors bind to the catalytic center interacting with two divalent metal ions simultaneously.

Diketo acids are known to work as potent inhibitors for divalent metal-related enzymes.¹⁶⁾ Therefore, diketo acid structure has served as a starting point for the design and optimization of inhibitors of HIV-1 integrase or influenza endonuclease. Pyrimidinol is another typical agent bearing a scaffold called *N*-hydroxyimide.¹⁷⁾ *N*-Hydroxyimides were firstly described as inhibitors of influenza endonuclease, but they also show a high potency in biochemical assays of HIV-1 RNase H. A natural product β -thujaplicinol is another scaffold and shows a high inhibitory potency for HIV-1 RNase H activity.¹⁸⁾

From an *in vitro* screening using 20000 chemical compounds, we found chemicals that blocked HIV-1 RT-associated RNase H activity.¹⁹⁾ The agents bearing the 5-nitro-furan-2-carboxylic acid ester moiety turned out to work as an RNase H inhibitor. Two of the agents were capable of suppressing HIV-1 replication in tissue culture. On the basis of the hit chemicals found in the screening, more than 50 derivatives of 5-nitro-furan-2-carboxylic acid were synthesized.²⁰⁾ Inhibitory potency of RNase H enzymatic activity was measured in a biochemical assay. Several derivatives showed higher

The authors declare no conflict of interest.

*To whom correspondence should be addressed. e-mail: hoshino@chiba-u.jp

© 2012 The Pharmaceutical Society of Japan

inhibitory activities than those of the hit chemicals. Modulation of the 5-nitro-furan-2-carboxylic moiety resulted in a decrease in inhibitory potency. In contrast, many derivatives with modulation of other parts maintained inhibitory activities. These studies indicate that the nitro-furan-carboxylic moiety is one of the potent scaffolds for RNase H inhibitor.

In this study, we further synthesized chemical compounds bearing the 5-nitro-furan-2-carboxylic acid ester moiety and examined the potency for anti-HIV drugs blocking RT-associated RNase H enzymatic activity. The potency of the synthesized compounds was evaluated through the measurement of inhibitory activity with real-time monitoring of fluorescence emission from the digested RNA substrate. In addition, the cytotoxicity of these compounds was assessed in 293T cells. Computer simulation with molecular dynamics (MD) method was also performed to analyze the stability of the binding structure of an active compound.

Experimental

Organic Synthesis Compound **1** was synthesized by creating an ester linkage between a nitro-furan carboxylic acid and an α -chloro-amide bound with benzyl and pentyl groups, by 3 h reaction at 60°C in dimethylformamide (DMF) in the presence of dimethyl-aminopyridine (DMAP). Chemical modulation was performed for the nitro-furan moiety, with changing the starting block from furan to thiophene or pyrrole *etc.* **2–8**. These compounds **2–8** were synthesized in the similar manner to compound **1**. The derivatives bearing 5-nitro-furan-2-ester scaffold, compounds **9–27**, were prepared by the reaction of converting 5-nitro-2-furoic acid into an acid chloride with thionyl chloride, followed by the nucleophilic substitution reaction in the presence of NEt_3 in tetrahydrofuran (THF) with setting the temperature at 0°C for the initial 30 min. and elevated it to r.t. afterward. Since a hydroxy group bound to phenyl ring is more reactive than a hydroxy group bound to alkane, the substitution reaction dominantly produced phenyl-ester linkage (**9–16**) when a nucleophilic reagent contained two hydroxy groups. When a nucleophilic reagent contained only one hydroxy group, the substitution reaction generated alkyl-ester linkage (**17–27**). Compounds **28–30** were produced by generating nitro-furan-carbonyl-alkyl-benzene through the reaction of Weinreb amides containing benzyl group with alkyl lithium, followed by incorporation of nitro group into the phenyl ring using white fuming nitric acid and acetic anhydride. Compounds **29** and **30** were separated by flash chromatography. Compounds **31–33** were generated by using hydroxy-amines as nucleophilic reagents.

Evaluation of Inhibitory Activity The 50% inhibitory concentration (IC_{50}) of the synthesized compounds for RT-associated RNase H activity was determined from the chemical concentration reducing the rate for substrate cleavage reaction to half relative to the control. A real-time monitoring assay was employed to estimate the IC_{50} .^{21,22} In short, two oligo-nucleotides were annealed at final concentrations of 2.5 and 0.25 μM for substrate. One was oligo-ribonucleotide 5'-GAUCUGAGCCUGGGAGCU-3' with 6-carboxy-fluorescein (FAM) conjugated at the 3' end, and the other was oligo-deoxyribonucleotide 5'-AGTCCCAGGCTCAGATC-3' with black hole quencher (BHQ) conjugated at the 5' end. Enzyme reaction with 100 ng RT, 0.025 μM oligo-ribonucleotide, and 0.25 μM oligo-deoxyribonucleotide was carried out in a volume

of 10 μL at 37°C. Fluorescence at 488 nm was monitored every 150 s using a multimode detector.

HIV-1 RT was expressed in *Escherichia coli* and purified by using a HiTrap Ni affinity column. The purified RT was dialyzed to reduce the concentration of imidazole from the elution buffer and then incubated with human rino virus (HRV) 3C protease to cleave an N-terminal hexahistidine tag. The protein was further purified by nickel-coordinated nitrilotriacetic acid (Ni-NTA) to remove the uncleaved protein and HRV 3C protease. The RT was dialyzed against a buffer of 50 mM Tris-HCl at pH 7.5 and 200 mM NaCl and was stored at -20°C with adding 50% (v/v) glycerol.

Assessment of Cytotoxicity 3-(4,5-Dimethylthiazol-2-yl)-2,5-diphenyltetrazolium bromide (MTT) assay was carried out with 293T cell line. First, 100 μL medium (RPMI-1640) supplemented with 10% fetal bovine serum (FBS) containing 2% dimethylsulfoxide (DMSO) was loaded in a 96-well plate, and 200 μL medium with 10% FBS and 2% DMSO containing test compounds at a concentration of 200 μM was added to the wells in the first column of the plate. Different concentrations of compound were prepared for the second, third and fourth columns. The final concentrations of these columns were 100, 50, 25 and 12.5 μM , respectively. Second, 100 μL 293T cells at a concentration of $2 \times 10^5/\text{mL}$ were added to the respective wells. The final concentration of DMSO in each well was 1%. Third, cells were incubated for 3 d at 37°C with 5% CO_2 atmosphere. A hundred micro liter of supernatant was removed from the cultured medium and 15 μL MTT reagent for dye solution was added to each well and the cells were incubated for 1 h. Then, 100 μL solution of stop mix was added, and the cells were incubated overnight at 4°C to sufficiently dissolve the dye. Finally, intensity of $\text{OD}_{570/690}$ was measured by a spectrofluorometer.

Molecular Dynamics Simulation A computational model of HIV-1 RT domain was constructed from an X-ray crystal structure with Protein Data Bank code 3QIO.²³ Atom coordinates for the missing residues were generated by using Modeller9.9.²⁴ According to the results of the recent X-ray crystallographic studies on the complex of RNase H domain and its inhibitors,^{25–27} the RNase H domain contains two divalent metal ions at the center of the active site. Two Mn^{2+} ions in the crystal structure were replaced with Mg^{2+} ions. The protonation states of all of the ionizable residues were predicted by PropKa program²⁸ in the presence of two Mg^{2+} ions at the active site. Atom charges of the compounds were determined from the electrostatic potential obtained from quantum chemical calculations, followed by the restrained electrostatic potential (RESP) fitting²⁹ in a similar manner to the previous studies.^{30–33} The atom charge for Mg^{2+} ion was setting to 1.54, which was also determined by the RESP method based on the calculated electrostatic potential obtained by QM/MM technique carried out in a similar manner to the previous work.²⁰ An active compound was combined with HIV-1 RT domain, referring the binding structure predicted in our previous work.²⁰ The compound-bound RT model was placed in a rectangular box and solvated with TIP3P water molecules,³⁴ with all of the crystal water molecules remaining. Periodic boundary conditions were applied to avoid the edge effect in all calculations.

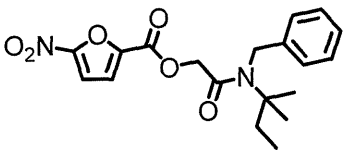
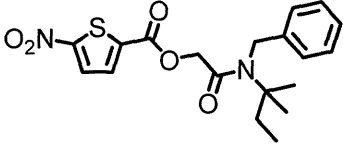
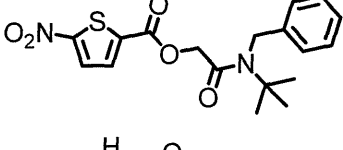
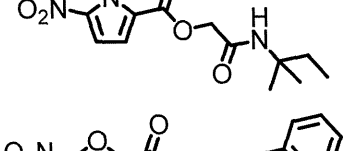
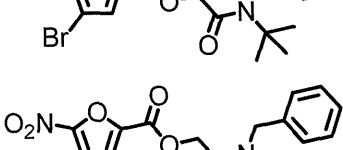
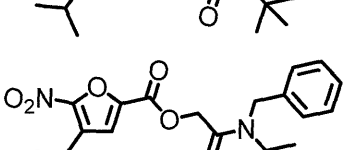
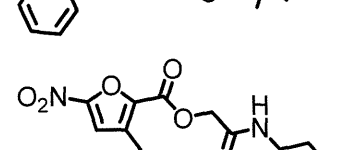
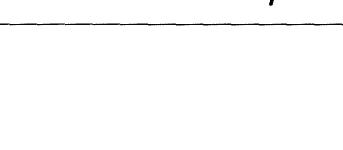
Minimizations and MD simulations were carried out using sander module of AMBER9.³⁵ The modified ff03 force field³⁶

was used as the parameters for molecular dynamics. The cut-off distance for the long range electrostatic and van der Waals energy terms was set to 12.0 Å. The expansion and shrinkage of all covalent bonds connecting to hydrogen atom were constrained using the SHAKE algorithm.³⁷⁾ Energy minimization was achieved in three steps. Initially, movement was allowed only for water molecules. Next, compound and divalent metal ions were allowed to move in addition to the water molecules. Finally, all atoms were allowed to move freely. In each step, energy minimization was executed by the steepest descent method for the first 10000 cycles and the conjugated gradient method for the subsequent 10000 cycles. After a 0.1 ns heating calculation until 310K using the NVT ensemble condition, a 20 ns equilibrating calculation was executed at 1.0 atm and at 310K under the NPT ensemble condition, with an integration time step of 2.0 fs.

Results

Eight analogues of 5-nitro-furan-2-carboxylic acid ester were synthesized by converting the 5-nitro-furan moiety into other functional groups and examined for their RNase H inhibitory activities (Table 1). Compound **1** has a typical chemical structure showing an inhibitory potency for HIV-1 RNase H enzymatic activity. This compound bears nitro-furan ester core connecting to the pentyl- and benzyl-bound amide group. Replacement of furan with thiophene largely decreased compound potency (**2**, **3**). Conversion of furan into pyrrole also resulted in complete loss of compound potency (**4**). Attaching a halogen to the 4th position of furan exhibited a slight increase of inhibitory activity (**5**), while a hydrophobic or aromatic substitute resulted in loss of inhibitory potency (**6**, **7**). Introduction of even a small hydrophobic group at the 3rd position of furan decreased inhibitory activity (**8**).

Table 1. RNase H Inhibitory Activity and Cytotoxicity of the Derivatives Modulated at Nitro-Furan Moiety

Compound	Structure	IC ₅₀ (μM)	CC ₅₀ (μM)
1		8.4	74
2		>50	49
3		30.3	50
4		>50	86
5		6.6	3
6		>50	>100
7		>50	>100
8		25.7	76

Eight derivatives bearing 5-nitro-furan phenyl ester core were examined as shown in Table 2. A similar degree of inhibitory activity was observed for the analogs having a hydroxy group at the *meta* or *para* position of phenyl ring (9–11). While substitution of the hydroxy group with acetyl group showed a similar degree of inhibitory activity (12), substitution with ethyl-ester increased compound potency (13). Further, introduction of methoxy group at the *ortho* position also increased compound potency (14). The compound containing methoxy-carbonyl and methoxy groups at the *para* or *ortho* positions exhibited a fine inhibitory activity (15). Introduction of phenyl-methyl-amine at the *para* position also maintained compound potency (16).

Eleven derivatives bearing 5-nitro-furan ester core bound with benzyl-based substitutes were investigated as summarized in Table 3. Connection of a benzyl group without any additional functional substitute showed moderate inhibitory activity (17). Attaching nitro group, methoxy-ether, or *tert*-butoxy-ester exhibited slight changes in compound potency (18–20). Extension of alkyl chain caused no significant difference in inhibitory potency (21). However, addition of hydroxy group decreased inhibitory activity (22). Introduction of methoxy group further decreased compound potency regardless of the position of the group bound to phenyl ring (23–25). While connection of two methoxy groups improved compound potency (26), replacement of two methoxy groups by chlorides showed low inhibitory activity (27).

Six derivatives were synthesized by changing the ester bond

Table 2. RNase H Inhibitory Activity and Cytotoxicity of the Derivatives Bearing Phenyl Ester Core

Compound	-O-R	IC ₅₀ (μM)	CC ₅₀ (μM)
9		7.2	>100
10		8.2	24
11		9.1	>100
12		8.7	49
13		3.6	>100
14		3.1	>100
15		1.4	>100
16		3.8	>100

with carbonyl group as shown in Table 4. Ester linkage is disadvantageous for medicine because esterase digests the linkage and the drug concentration in a body decreases rapidly. Nitro-phenyl group was connected to the carbonyl carbon with changing the length of alkyl chain and the position of nitro group (28–30). None of the derivatives showed noticeable inhibitory activity. The ester linkage was replaced by an amide bond (31–33), in which hydroxy-methyl-benzyl, acetyl-methyl-benzyl, or bromo-methyl-benzyl was bound *via* a carbamoyl group. This modification also resulted in complete loss of compound potency.

Cytotoxicity was little or undetectable for most of the derivatives modulated at the nitro-furan moiety except for compound 5 (Table 1). No detectable cytotoxicity was also observed for most of the derivatives bearing nitro-furan-phenyl ester core (Table 2). It should be noted that highly active compounds, 14 and 15, showed no noticeable cytotoxicity at a concentration of 100 μM. In contrast, the analogs bearing ester core bound with benzyl-based substitute showed some degree of cytotoxicity (Table 3). Further, the analogs converted the ester into amide or ketone showed cytotoxicity in which CC₅₀ ranged from 9 to 32 μM (Table 4). Overall, in the measurement using 293T cells, half of the synthesized compounds showed noticeable cytotoxicity but almost all of the toxicity-detected compounds showed little RNase H inhibitory activity. Accordingly, the results of this assay suggest that active compounds have no significant cytotoxicity and the nitro-furan-phenyl ester skeleton is the most favorable among them from a cytotoxic viewpoint.

In order to examine the stability of the binding structure of a potent compound inside the active site of the target protein, MD simulation was performed for the complex of a synthesized derivative 15 and RNase H domain. MD simulation was carried out for 20 ns and root mean square deviation (RMSD) relative to the structure after heating was calculated as shown in Fig. S1 of the supplemental information. The RMSD value showed a gradual increase up to 5 ns and scarcely changed during later 15 ns. Accordingly, the binding conformation of the complex was judged to be equilibrated. In order to extract the snapshot structure representing a typical binding mode of compound 15 and RNase H domain, the averaged structure was obtained using 2500 trajectories from the last 5 ns of MD simulation. The RMSD between each trajectory and the average structure was calculated, and then one trajectory with the smallest RMSD value was determined to be the typical complex structure shown in Fig. 1a.

Two Mg²⁺ ions were held by the side chains of four acid residues; Asp443, Glu478, Asp498, Asp549, and the compound was stably bound to the active site without changing the binding mode during 20 ns simulation. In the binding structure, the nitro-furan-ester core is especially, stably bound to two Mg²⁺ ions as shown in Fig. 1a. A stereo view of the binding structure is presented in Fig. S2 of the supplemental information. The oxygen atom on the furan ring is oriented toward the divalent metals. Nitro oxygen and carbonyl oxygen of the ester are strongly coordinated to the respective Mg²⁺ ions. Therefore, a large ring-shaped configuration of -Mg-O-N-C-O-C-C-O-Mg- is formed. The inter-atomic distance between two Mg²⁺ ions is 3.8 Å. The distance between the nitro oxygen atom and one Mg²⁺ ion is 1.9 Å, and that between carbonyl oxygen and the other Mg²⁺ ion is also 1.9 Å. Figure

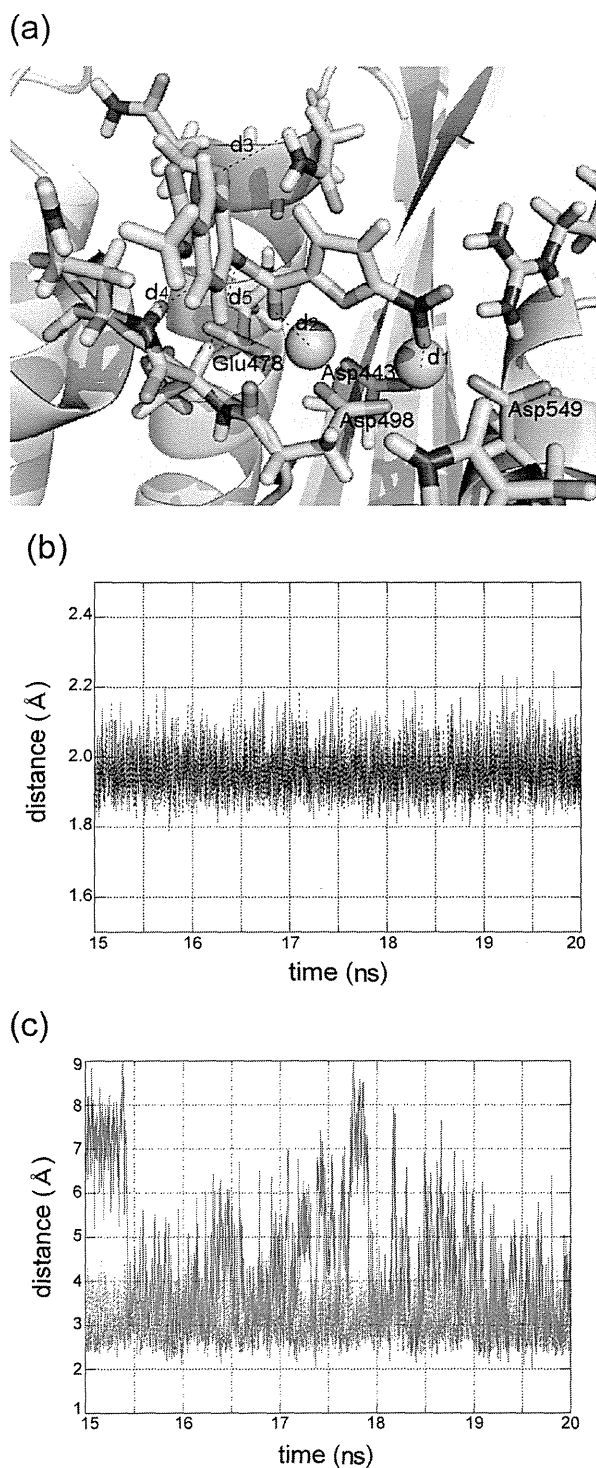


Fig. 1. (a) Binding Structure of an Active Compound to the RNase H Domain, Obtained by MD Simulation

Compound and several polar residues are shown in stick representation. Two Mg^{2+} ions are denoted by spheres. (b) Changes in the distances between nitro oxygen and Mg^{2+} ion (d_3 ; red solid line) and between carbonyl oxygen and another Mg^{2+} ion (d_2 ; blue dotted line) for the last 5 ns of MD simulation. (c) Changes in the distances between methoxy oxygen and amino hydrogen of Asn474 (d_3 ; green solid line), between ester oxygen and amide hydrogen of main chain of Gln500 (d_4 ; cyan broken line), and between ester oxygen and $C\alpha$ hydrogen of Ser499 (d_5 ; yellow dotted line) for the last 5 ns of MD simulation. Color images were converted into gray scale; red solid line, blue dotted line, green solid line, cyan broken line, yellow dotted line have been converted into gray scale.

1b shows the changes of these two distances for the last 5 ns of MD simulation. These graphs clearly indicate that the interaction of oxygen atom and Mg^{2+} ion is quite strong and that the oxygen–Mg interaction is essentially important for the binding of potent compound.

Methoxy-carbonyl and methoxy groups connected to phenyl stick out from the binding pocket. The distance between methoxy oxygen and hydrogen atom of amino group of Asn474 was monitored as shown in Fig. 1c. The distance largely fluctuates during the simulation and the interaction is not so steady. Hence, there is much room for improvement in this region. The oxygen atom at the ester bond has noticeable interactions with the amide group of main chain of Gln500. The change of the distance between the ester oxygen and the hydrogen atom of the amide group is shown in Fig. 1c. No abrupt, large change is observed in the distance. Therefore, the interaction contributes to stabilizing the binding of the potent compound. The distance between the ester oxygen and the $C\alpha$ hydrogen atom of Ser 499 was also monitored. The distance shows no large change for the last 5 ns of simulation, which suggests the stability of the binding of the ester part with RNase H domain. Consequently, it is confirmed from the MD simulation that an active compound **15** is stably bound to the active site of the RNase H domain with coordinating to two divalent metal ions and making supportive interaction at the ester part.

Discussion

According to the data summarized in Table 3, it is suggested that various kinds of functional groups connected to the benzyl ring have little interaction with the RNase H domain and that the functional group-binding region is located outside the binding pocket and is exposed to the solvent. Further, a comparison of inhibitory activity between compounds **17–20** and compounds **21–27** suggests that the length of alkyl chain connecting to phenyl ring has a significant influence on the difference in compound potency. That is, the longer alkyl chain in compounds **21–27** is less favorable in terms of both inhibitory activity and cytotoxicity. This indicates that a strategy to increase the inhibitory activity is to position the substitute closer to the nitro-furan group. The conversion may allow the aromatic ring or substitute to interact with the target protein inside the binding pocket.

A comparison of inhibitory activities of compounds in Tables 2 and 3 indicates that the introduction of phenyl-ester connected to nitro-furan shows higher compound potency than that of benzyl-ester. This is consistent with the findings described above paragraph and supports the notion that the compound potency increases when the position of the substitute connected to the ester linkage is closer to the nitro-furan. The incorporation of polarized substitutes like methoxy, hydroxy, methoxy-carbonyl, or ethoxy-carbonyl group is effective to increase the compound potency. In particular, the introduction of methoxy group at the *ortho*-position of phenyl ring effectively increases the inhibitory activity.

All the compounds in Tables 2 and 3 have the ester linkage. The data summarized in Table 4 clearly indicate that conversion of the ester linkage into carbonyl and/or amide bond results in loss of inhibitory potency. Both bonds will be likely to make the chemical to be in a straight configuration. If a compound has a straight form, the side part of the compound

Table 3. RNase H Inhibitory Activity and Cytotoxicity of the Derivatives Bearing Ester Core Bound with Benzyl-Based Substitute


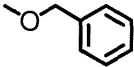
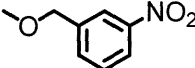
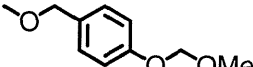
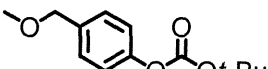
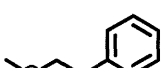
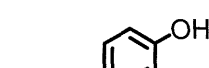
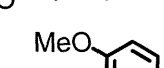
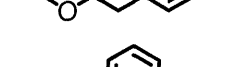
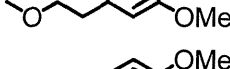
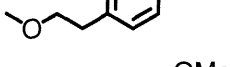
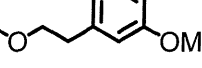
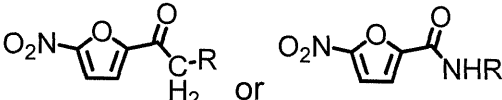
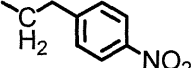
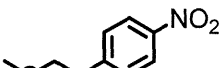
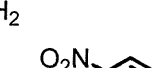
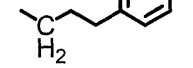
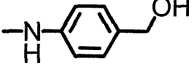
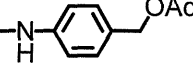
			
Compound	-O-R	IC ₅₀ (μM)	CC ₅₀ (μM)
17		5.4	38
18		5.0	>100
19		5.8	75
20		4.5	>100
21		5.1	57
22		7.9	39
23		14.2	42
24		18.6	36
25		12.5	36
26		8.5	51
27		17.4	64

Table 4. RNase H Inhibitory Activity and Cytotoxicity of the Derivatives Converted the Ester Bond into Other Kinds of Linkages

			
Compound	-CH ₂ -R or -NH-R	IC ₅₀ (μM)	CC ₅₀ (μM)
28		>50	11
29		>50	17
30		>50	9
31		>50	29
32		>50	27
33		>50	32

RNase H reaction site to exert its enzymatic activity.⁴⁰⁾ A theoretical study by De Vivo *et al.* suggested that the presence of two divalent metal ions is essential for RNase H activity and that two metal ions act cooperatively with facilitating the binding of a substrate and catalyzing the enzymatic reaction.⁴¹⁾ This theoretical finding strongly suggests double coordination of divalent metal ions at the RNase H domain. Crystal structures on the complex of the RNase H domain and its inhibitor were successively reported from three different research groups.^{23,25-27)} All of the crystal structures ever reported showed the presence of two metal ions at the active site. One of the divalent metal ions was held deep inside the binding pocket of the RT RNase H domain with making coordination bonds to three carboxyl groups of Asp443, Glu478 and Asp498. The other was fixed with making coordination bonds to two carboxyl groups of Asp443 and Asp549. The distance between two metal ions was about 4 Å. Every inhibitor in crystal structures was revealed to have a similar binding mode. That is, inhibitors are stabilized with forming coordination bonds to both metal ions. Accordingly, it is highly probable that the chemical compounds showing RNase H inhibitory activity examined in this study are also coordinated to two divalent metal ions. Hence, negatively charged oxygen atoms of the nitro group, furan, and carbonyl group are aligned in a straight form. This negatively charged region will be attached to the divalent metal ions.

The binding structure deduced from MD simulation indicates that ether oxygen at the ester bond has an interaction with a polar residue, Ser499, which is located at the deep inside of RNase H domain. This residue would have little

will collide with the inside wall of the binding pocket of the RNase H domain. Accordingly, compounds are hardly combined with the binding pocket.

The conversion of the nitro-furan group into pyrrole drastically decreases the inhibitory activity while conversion to nitro-thiophen maintains the activity (Table 1). This indicates that a nitro-furan or nitro-thiophene core is indispensable for inhibitory potency. The characteristic property of nitro-furan is its large electric polarity. Oxygen atoms are negatively charged and these oxygen atoms will be coordinated to divalent metal ions at the RNase H active site. The attachment of non-polar substitute to furan results in decrease of compound potency. Accordingly, the 3rd and 4th positions of furan become close to the residues inside the RNase H active site.

RNase H of HIV-1 exerts its enzymatic activity by incorporating divalent metal ions at the reaction site.^{38,39)} It had been controversial how many metal ions were required at the

influence on the function of RNase H. Therefore, one of the designs to improve inhibitory activity is to modify the compound to bear some polar functional group that enables a strong interaction with Ser499. In order to enhance the binding affinity of the compounds with RNase H active site, the incorporation of a polar functional group bound to phenyl ring is one of the possible conversions of our derivatives. The distance between methoxy group and the amine of Asn474 largely fluctuated during MD simulation. If the interaction with Asn474 is enforced, compound will be more stably combined with the RNase H domain.

Conclusion

More than 30 chemical compounds were synthesized for developing the inhibitors of RNase H activity of HIV-1 reverse transcriptase. Inhibitory potency of RNase H enzymatic activity was measured in a biochemical assay with a real-time fluorescence monitoring method. The active compounds found in our previous studies commonly bear nitro-furan ring connecting to hydrophobic region *via* an ester linkage. Conversion of the nitro-furan group into pyrrole drastically decreased the inhibitory activity while conversion into nitro-thiophene maintained the compound potency. This means that the structural basis of nitro-furan or nitro-thiophene is indispensable for inhibitory activity. An improvement in compound potency was observed when a phenyl-ester moiety was connected to the nitro-furan and further methoxy-carbonyl and methoxy groups were bound to the phenyl ring. No notable change in inhibitory potency was observed when benzyl-ester based substitute was connected to nitro-furan. Modulation of ester linkage resulted in complete loss of compound potency. Molecular dynamics simulation was performed to examine the stability of the binding structure of a synthesized active compound to RNase H domain. It was demonstrated that a potent compound was stably bound to the active site with establishing strong coordinate bonds with divalent metal ions located at the active site. The present study provides important information for designing prospective chemical structures inhibiting HIV-1 RNase H activity.

Acknowledgments This work was supported by a Health and Labor Science Research Grant for Research on Publicly Essential Drugs and Medical Devices from the Ministry of Health and Labor of Japan. A part of this work was also supported by a Grant-in-Aid for Scientific Research (C) from Japan Society for the Promotion of Science (JSPS). Theoretical calculations were performed at the Research Center for Computational Science, Okazaki, Japan and at the Information Technology Center of the University of Tokyo and also by the high-performance computer system at Institute for Media Information Technology in Chiba University.

References

- Goody R. S., Müller B., Restle T., *FEBS Lett.*, **291**, 1–5 (1991).
- Ren J., Stammers D. K., *Virus Res.*, **134**, 157–170 (2008).
- Andréola M. L., De Soultrait V. R., Fournier M., Parissi V., Desjoubert C., Litvak S., *Expert Opin. Ther. Targets*, **6**, 433–446 (2002).
- Klumpp K., Mirzadegan T., *Curr. Pharm. Des.*, **12**, 1909–1922 (2006).
- Tramontano E., *Mini Rev. Med. Chem.*, **6**, 727–737 (2006).
- Tanese N., Telesnitsky A., Goff S. P., *J. Virol.*, **65**, 4387–4397 (1991).
- Telesnitsky A., Goff S. P., *EMBO J.*, **12**, 4433–4438 (1993).
- Borkow G., Fletcher R. S., Barnard J., Arion D., Motakis D., Dmitrienko G. I., Parniak M. A., *Biochemistry*, **36**, 3179–3185 (1997).
- Tramontano E., Esposito F., Badas R., Di Santo R., Costi R., La Colla P., *Antiviral Res.*, **65**, 117–124 (2005).
- Tarrago-Litvak L., Andreola M. L., Fournier M., Nevinsky G. A., Parissi V., de Soultrait V. R., Litvak S., *Curr. Pharm. Des.*, **8**, 595–614 (2002).
- Cowan J. A., Ohyama T., Howard K., Rausch J. W., Cowan S. M., Le Grice S. F., *J. Biol. Inorg. Chem.*, **5**, 67–74 (2000).
- Haren L., Ton-Hoang B., Chandler M., *Annu. Rev. Microbiol.*, **53**, 245–281 (1999).
- Steitz T. A., Smerdon S. J., Jäger J., Joyce C. M., *Science*, **266**, 2022–2025 (1994).
- Nowotny M., Gaidamakov S. A., Crouch R. J., Yang W., *Cell*, **121**, 1005–1016 (2005).
- Nowotny M., Gaidamakov S. A., Crouch R. J., Yang W., *EMBO J.*, **25**, 1924–1933 (2006).
- Shaw-Reid C. A., Munshi V., Graham P., Wolfe A., Witmer M., Danzeisen R., Olsen D. B., Carroll S. S., Embrey M., Wai J. S., Miller M. D., Cole J. L., Hazuda D. J., *J. Biochem.*, **278**, 2777–2780 (2003).
- Hang J. Q., Rajendran S., Yang Y., Li Y., In P. W. K., Overton H., Parkes K. E. B., Cammack N., Martin J. A., Klumpp K., *Biochem. Biophys. Res. Commun.*, **317**, 321–329 (2004).
- Budihis S. R., Gorshkova I., Gaidamakov S., Wamiru A., Bona M. K., Parniak M. A., Crouch R. J., McMahon J. B., Beutler J. A., Le Grice S. F., *Nucleic Acids Res.*, **33**, 1249–1256 (2005).
- Fuji H., Urano E., Futahashi Y., Hamatake M., Tatsumi J., Hoshino T., Morikawa Y., Yamamoto N., Komano J., *J. Med. Chem.*, **52**, 1380–1387 (2009).
- Yanagita H., Urano E., Matsumoto K., Ichikawa R., Takaesu Y., Ogata M., Murakami T., Wu H. G., Chiba J., Komano J., Hoshino T., *Bioorg. Med. Chem.*, **19**, 816–825 (2011).
- Chan K. C., Budihis S. R., Le Grice S. F., Parniak M. A., Crouch R. J., Gaidamakov S. A., Isaaq H. J., Wamiru A., McMahon J. B., Beutler J. A., *Anal. Biochem.*, **331**, 296–302 (2004).
- Parniak M. A., Min K. L., Budihis S. R., Le Grice S. F., Beutler J. A., *Anal. Biochem.*, **322**, 33–39 (2003).
- Lansdon E. B., Liu Q., Leavitt S. A., Balakrishnan M., Perry J. K., Lancaster-Moyer C., Kutty N., Liu X., Squires N. H., Watkins W. J., Kirschberg T. A., *Antimicrob. Agents Chemother.*, **55**, 2905–2915 (2011).
- Martí-Renom M. A., Stuart A. C., Fiser A., Sánchez R., Melo F., Sali A., *Annu. Rev. Biophys. Biomol. Struct.*, **29**, 291–325 (2000).
- Kirschberg T. A., Balakrishnan M., Squires N. H., Barnes T., Brenda K. M., Chen X., Eisenberg E. J., Jin W., Kutty N., Leavitt S., Liclican A., Liu Q., Liu X., Mak J., Perry J. K., Wang M., Watkins W. J., Lansdon E. B., *J. Med. Chem.*, **52**, 5781–5784 (2009).
- Himmel D. M., Maegley K. A., Pauly T. A., Bauman J. D., Das K., Dharia C., Clark A. D. Jr., Ryan K., Hickey M. J., Love R. A., Hughes S. H., Bergqvist S., Arnold E., *Structure*, **17**, 1625–1635 (2009).
- Su H. P., Yan Y., Prasad G. S., Smith R. F., Daniels C. L., Abeywickrema P. D., Reid J. C., Loughran H. M., Kornienko M., Sharma S., Grobler J. A., Xu B., Sardana V., Allison T. J., Williams P. D., Darke P. L., Hazuda D. J., Munshi S., *J. Virol.*, **84**, 7625–7633 (2010).
- Li H., Robertson A. D., Jensen J. H., *Proteins*, **61**, 704–721 (2005).
- Cieplak P., Cornell W. D., Bayly C., Kollman P. A., *J. Comput. Chem.*, **16**, 1357–1377 (1995).
- Matsuyama S., Aydan A., Ode H., Hata M., Sugiura W., Hoshino T., *J. Phys. Chem. B*, **114**, 521–530 (2010).
- Sano E., Li W., Yuki H., Liu X., Furihata T., Kobayashi K., Chiba K., Neya S., Hoshino T., *J. Comput. Chem.*, **31**, 2746–2758 (2010).

- 32) Ode H., Neya S., Hata M., Sugiura W., Hoshino T., *J. Am. Chem. Soc.*, **128**, 7887–7895 (2006).
- 33) Ode H., Matsuyama S., Hata M., Neya S., Kakizawa J., Sugiura W., Hoshino T., *J. Mol. Biol.*, **370**, 598–607 (2007).
- 34) Jorgensen W. L., Chandrasekhar J., Madura J. D., Impey R. W., Klein M. L., *J. Chem. Phys.*, **79**, 926–935 (1983).
- 35) Case D. A., Darden T. A., Cheatham T. E. III, Simmerling C. L., Wang J., Duke R. E., Luo R., Merz K. M., Pearlman D. A., Crowley M., Walker R. C., Zhang W., Wang B., Hayik S., Roitberg A., Seabra G., Wong K. F., Paesani F., Wu X., Brozell S., Tsui V., Gohlke H., Yang L., Tan C., Mongan J., Hornak V., Cui G., Beroza P., Mathews D. H., Schafmeister C., Ross W. S., Kollman P. A., “AMBER 9,” University of California, San Francisco, 2006.
- 36) Katagiri D., Fuji H., Neya S., Hoshino T., *J. Comput. Chem.*, **29**, 1930–1944 (2008).
- 37) Ryckaert J.-P., Ciccotti G., Berendsen H. J. C., *J. Comput. Phys.*, **23**, 327–341 (1977).
- 38) Sarafianos S. G., Das K., Tantillo C., Clark A. D. Jr., Ding J., Whitcomb J. M., Boyer P. L., Hughes S. H., Arnold E., *EMBO J.*, **20**, 1449–1461 (2001).
- 39) Huang H., Chopra R., Verdine G. L., Harrison S. C., *Science*, **282**, 1669–1675 (1998).
- 40) Klumpp K., Hang J. Q., Rajendran S., Yang Y., Derosier A., Wong Kai In P., Overton H., Parkes K. E., Cammack N., Martin J. A., *Nucleic Acids Res.*, **31**, 6852–6859 (2003).
- 41) De Vivo M., Dal Peraro M., Klein M. L., *J. Am. Chem. Soc.*, **130**, 10955–10962 (2008).

Mechanism of Drug Resistance of Hemagglutinin of Influenza Virus and Potent Scaffolds Inhibiting Its Function

Hiroshi Yanagita,^{†,#} Norio Yamamoto,^{‡,§,#,*} Hideyoshi Fuji,[†] Xinli Liu,[†] Masakazu Ogata,[†] Mizuho Yokota,[†] Hiroshi Takaku,^{||} Hideki Hasegawa,[⊥] Takato Odagiri,[‡] Masato Tashiro,[‡] and Tyuji Hoshino^{†,*}

[†]Graduate School of Pharmaceutical Sciences, Chiba University, Inohana 1-8-1, Chuo-ku, Chiba 260-8675, Japan

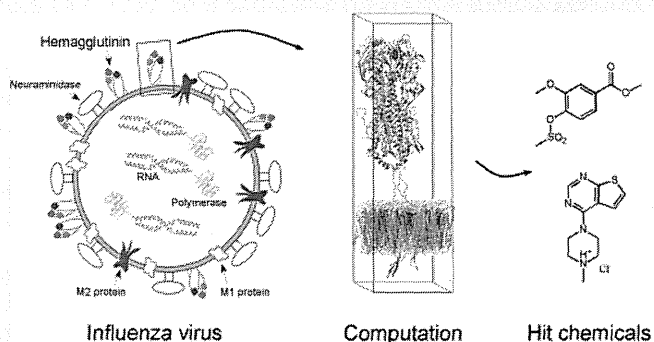
[‡]Influenza Virus Research Center and [⊥]Department of Pathology, National Institute of Infectious Diseases, 4-7-1 Gakuen, Musashimurayama, Tokyo 208-0011, Japan

[§]Department of General Medicine, Juntendo University School of Medicine, 2-1-1 Hongo, Bunkyo-ku, Tokyo 113-8421, Japan

^{||}Department of Life and Environmental Science, Chiba Institute of Technology, 2-17-1 Tsudanuma, Narashino-shi, Chiba 275-0016, Japan

Supporting Information

ABSTRACT: Highly pathogenic influenza viruses have become a global threat to humans. It is important to select an effective therapeutic option suitable for the subtypes in an epidemic or pandemic. To increase the options, the development of novel antiviral agents acting on targets different from those of the currently approved drugs is required. In this study, we performed molecular dynamics simulations on a spike protein on the viral envelop, hemagglutinin, for the wild-type and three kinds of mutants using a model system consisting of a trimeric hemagglutinin complex, viral lipid membrane, solvation waters, and ions. A natural product, stachyflin, which shows a high level of antiviral activity specific to some subtypes of influenza viruses, was examined on binding to the wild-type hemagglutinin by docking simulation. The compound potency of stachyflin is, however, easily lost due to resistant mutations. From a comparison of simulation results between the wild-type and the resistant mutants, the reason for the drug resistance of hemagglutinin was clarified. Next, 8 compounds were selected from a chemical database by *in silico* screening, considering the findings from the simulations. Inhibitory activities to suppress the proliferation of influenza virus were measured by cell-based antiviral assays, and two chemical scaffolds were found to be potent for an inhibitor. More than 30 derivatives bearing either of these two chemical scaffolds were synthesized, and cell culture assays were carried out to evaluate the compound potency. Several derivatives displayed a high compound potency, and 50% effective concentrations of two synthesized compounds were below 1 μM .



Influenza viruses cause acute respiratory infection in humans that occasionally progresses to a severe pulmonary condition. Even seasonal epidemics account for 300,000 or more deaths per a year all over the world. Recently, the emergence of highly pathogenic avian and swine influenza viruses has become a global threat to humans. Avian influenza H5N1 virus infections have been reported since 2003,¹ and a pandemic of transmissible H5N1 virus is a serious concern for public health.² The recent outbreak of swine influenza subtype H1N1 resulted in considerable mortalities for infants and the elderly. While several anti-influenza drugs are currently approved, their effectiveness for pandemic viruses may be limited due to drug resistance. Therefore, the development of additional antiviral agents against influenza virus infection is needed.

The currently available anti-influenza drugs target one of two viral proteins: M2 protein and neuraminidase. M2 protein is embedded in the lipid membrane of the viral envelope and functions as an ion channel to pump protons into the viral particles. Amantadine and Rimantadine block the function of M2 protein by combining at the center of the channel or the side domain of this enzyme.^{3,4} Neuraminidase is a kind of spike protein sticking out on the viral particle surface. Neuraminidase causes the hydrolysis of neuraminic acid of the glycan of the host cell. Zanamivir, Oseltamivir, Peramivir, and Laninamivir have been used as neuraminidase inhibitors.^{5,6} Emergence of drug-resistant viruses has been reported for the above approved

Received: September 1, 2011

Accepted: January 4, 2012

Published: January 4, 2012

drugs. For example, resistance against Amantadine and Rimantadine was shown in the H3N2 and H1N1 viruses, and resistance against Oseltamivir was shown for the H1N1 virus.^{7–9} Since an RNA virus easily acquires amino acid mutations, the emergence rate of drug-resistant viruses is high. A drug-resistant virus is a serious issue in infectious diseases because a chemotherapeutic approach is restricted. In order to combat drug-resistant viruses, it is important to prepare many chemotherapeutic options and select an effective option suitable for subtypes in an epidemic. Accordingly, development of novel antiviral drugs that act on a target different from those of the currently approved drugs is needed.

A species of moss, *Stachybotrys* s. RF-7260, generates a unique natural product named stachyflin. Stachyflin was found to have strong antiviral activity against some subtypes of influenza viruses.^{10–12} The inhibitory mechanism of stachyflin is different from the inhibitory mechanism of the currently approved anti-influenza drugs. Stachyflin binds with hemagglutinin (HA) on the viral envelope and blocks conformation change of HA to prevent the lipid membrane of the viral envelope from merging with that of host cell. HA is one of the attractive targets of antiviral agents for the following reasons. First, HA is a key component in the viral infusioin process that has no cellular counterparts and therefore has a potential advantage in selectivity and toxicity. Second, HA inhibitors will complement other currently approved drugs since they act on a different molecular target in the virus life cycle.

Stachyflin is highly effective for influenza virus of A/WSN/33 H1N1 subtype, and the 50% inhibitory concentration (IC₅₀) value for the WSN strain was reported to be 3 nM.¹² However, its inhibitory activity for other strains including other H1N1 virus strains is not so high, and its inhibitory activity is easily decreased by amino acid mutations of the virus. Since several amino acid mutations involved in drug resistance are not localized in one domain of HA, it is difficult to understand the mechanism of drug resistance caused by mutations straightforwardly. The chemical structure of stachyflin is complicated. Five rings merge to form a structure called the 3*H*-naphthopyrano-isoindol-3-one scaffold, and stachyflin also contains five chiral centers (Figure 1a). This complexity in its chemical structure is another reason for the difficulty in improving compound potency for stachyflin derivatives.

Yoshimoto and co-workers performed an experiment on resistance induction with stachyflin¹³ and demonstrated that K51R, K121E, S206L in the HA2 subunit and V176I in the HA1 subunit appeared in resistant viruses (Figure 1b). K51R and K121E mutations were suggested to be essential for drug resistance. They suggested from a docking simulation that stachyflin was bound to a position close to Lys51 or Phe110 of HA. This simulation, however, provided no clear explanation for the mechanism of drug resistance due to the above amino acid mutations. The mechanism of the drug resistance of HA should be clarified for producing promising inhibitory compounds.

In this study, we performed computational analysis, screening to find candidate compounds, a cell-based antiviral assay, and synthesis of analogue compounds in the following manner: (1) Molecular dynamics (MD) simulations were carried out for the wild-type and three kinds of variants containing amino acid mutations responsible for drug resistance in order to clarify the mechanism. (2) A point for designing a potential inhibitor was deduced from the concept of minimizing the influence of the drug-resistance-related conformational change of HA. (3) An *in*

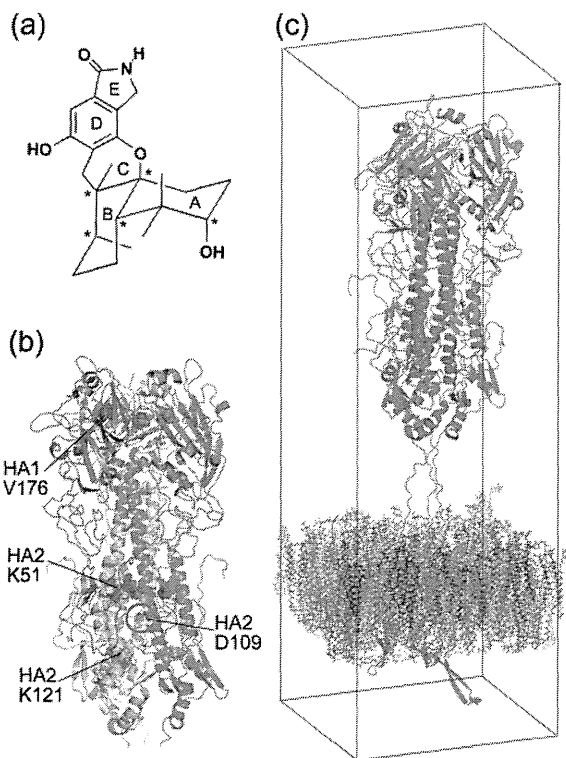


Figure 1. (a) Chemical structure of stachyflin. Stachyflin is composed of five complex rings and contains five chiral centers. The rings are labeled A–E, and chiral carbon atoms are marked by asterisks. (b) Structure of hemagglutinin in a trimer conformation. Spheres denote the residues introducing amino mutations in the respective mutants. The center residue targeted in the ligand docking simulation is indicated by a circle. (c) Calculation model of a complex of hemagglutinin trimer and lipid membrane. Hemagglutinin subunits HA1 and HA2 are colored blue and green, respectively. The membrane consists of 6 different kinds of lipid molecules, and its composition is presented in Supplementary Table S1. No water molecules or ions are shown for visual clarity.

silico screening was performed to find low-molecular-weight compounds showing inhibitory activity against HA, considering the above point and using the pharmacophore of stachyflin. (4) A cell-based assay was carried out to evaluate the inhibitory potencies of the compounds collected by the *in silico* screening. (5) Derivatives of the hit compounds found from the screening were synthesized, and their inhibitory activities were measured to elucidate the antiviral potency of the scaffold proposed in this work.

RESULTS AND DISCUSSION

Structural Difference in HA between the Wild-Type and Mutants. MD simulation was carried out for 30 ns to obtain the probable protein structure of HA in a trimer form for the wild-type and three mutants, using the model system containing a trimeric hemagglutinin and viral lipid membrane as shown in Figure 1c. The respective mutants contain the resistant mutations K51R and K121E in HA2 for mutant 1, V176I in HA1 and K51R, K121E in HA2 for mutant 2, and V176I in HA1 and K51R in HA2 for mutant 3. Root mean square deviation (rmsd) relative to the structure after heating is shown in Supplementary Figure S1. The rmsd value for the wild-type (Figure S1a) was scarcely changed during 30 ns. Each of the rmsd curves for the mutants (Figures S1b–d) shows a